C.D.I. REPORT NO. 88-05

VORTEX DYNAMICS

FOR

ROTORCRAFT INTERACTIONAL AERODYNAMICS

Prepared by

Todd R. Quackenbush

CONTINUUM DYNAMICS, INC.
P.O. BOX 3073
PRINCETON, NEW JERSEY 08543

and

Donald B. Bliss

DUKE UNIVERSITY
DURHAM, NORTH CAROLINA 27706

Prepared under SBIR Phase I Contract No. DAAL03-87-C-0013 for

DEPARTMENT OF THE ARMY
ARMY RESEARCH OFFICE
P.O. BOX 12211
RESEARCH TRIANGLE PARK, NORTH CAROLINA 27709

Approved by

Alan J. Bilanin

Alan J. Bilanin

March 1988

SUMMARY

The principal objective of this work was to explore the applicability of recent innovations in the analysis of vortex dynamics to problems of interest in rotorcraft interactional aerodynamics. Promising results were obtained in this exploratory work that indicate that these new techniques could be used as the foundation of a general analysis of rotor/airframe interactions.

The first topic addressed was the prediction of the velocity field downstream of helicopter rotors. Using a novel, full-span rotor wake representation constructed of curved vortex elements, accurate qualitative and quantitative predictions of wake velocity data were achieved for rotors in both low- and high-speed forward flight. The flow field predictions illustrated the radical changes that take place in the wake velocity field as speed increases and demonstrated the success of this new approach in capturing these variations.

Also, new methods for analyzing close interactions between vortices and fixed surfaces have been developed. The basis of this new approach is the inclusion of a special treatment of the vortex velocity field for close interactions with paneled surfaces which obviates the need for high local panel density. Model problems were solved featuring vortices in close proximity to flat surfaces and cylinders that amply illustrate the accuracy and efficiency of the new method.

The principal potential application for these new technologies is as building blocks for a more complete, general analysis of rotorcraft interactional aerodynamics. The results of this preliminary effort demonstrated that several additional features must be added to the current analyses to produce a flexible and generally applicable interaction analysis. Prominent among these were appropriate provision for the wake of nonlifting components such as the rotor hub, modeling of viscous effects in close vortex/surface interactions, and coupling of the new methods described above to appropriately modified aerodynamic panel codes. The primary conclusion of this research, however, is that the new techniques described herein can form the foundation of such an analysis.

TABLE OF CONTENTS

1. INTRODUCTION

1.1 Background

Historically, most of the analytical and computational work in rotorcraft wake modeling has focussed on prediction of isolated rotor performance and loads (Refs. 1-3). Substantial progress in this area has been made, including recent advances in the prediction of rotor loads and wake geometry using free wake models at Continuum Dynamics, Inc. (Refs. 4 and 5). However, treatment of main rotor wake effects on other components of the helicopter (e.g., the tail rotor, empennage, and fuselage) is much less advanced. Thus, a significant opportunity exists to exploit current and anticipated developments in rotor wake modeling to advance the current understanding of interactional aerodynamics.

The importance of having a reliable tool to predict such loads is amply illustrated in a review of the literature. Wiesner and Kohler (Ref. 6) for example, cite the important effects on tail rotor thrust and power of the rolling-up vortices from the main rotor wake. This reference also notes the large download imposed by the main rotor wake on the fixed horizontal stabilizer in forward flight.

An extensive investigation of interactional aerodynamic effects in single-rotor helicopters by Sheridan, et al (Refs. 7 and 8) in the Boeing V/STOL wind tunnel, points out still more phenomena of significance. For instance, a strong sensitivity of vertical fin side force to main rotor wake impingement was noted in Ref. 8; both wind azimuth and main rotor thrust were found to be important parameters with the tail rotor on or off. Also, the effect of the main rotor wake on tail rotor collective requirements is well documented; Figure 1 shows the large excursions in right- and left-quartering flight due to main rotor wake impingement.

Subsequent wind tunnel studies (Ref. 9) of a model of a OH-58 indicated that the impingement of the main rotor wake on the vertical fin played an

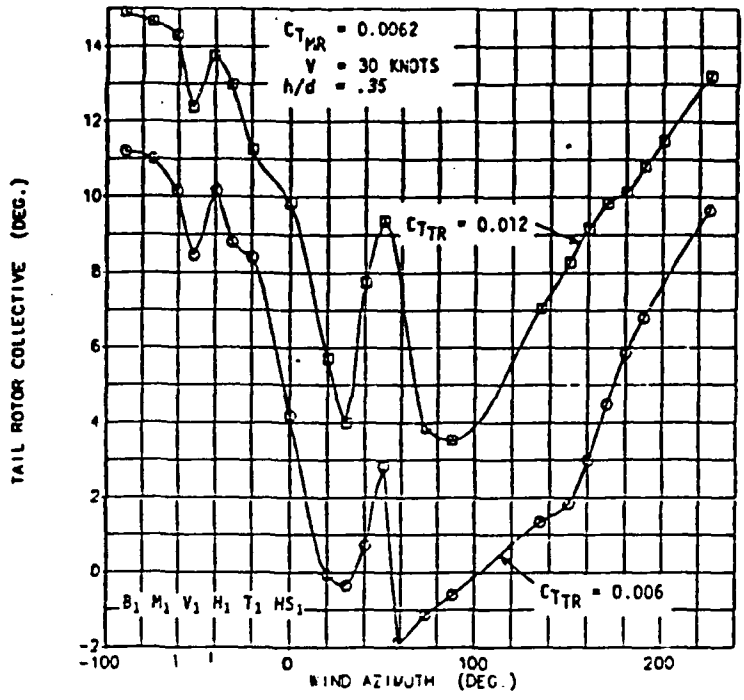

Figure 1. Tail rotor collective required for fixed thrust at low forward speed (Ref. 8).

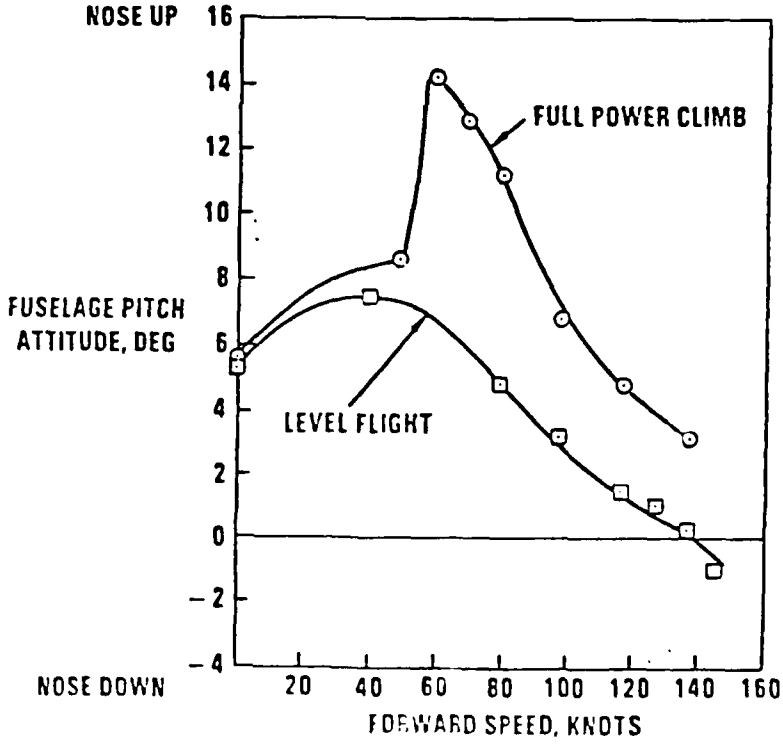

Figure 2. AH-64 pitch attitude excursions due to main rotor downwash on horizontal stabilizer (Ref. 10).

important role in determining the adverse fin forces which, in turn, degrade the directional control margin of the aircraft. In the low speed region below 20 knots, the dominance of the main rotor downwash serves to limit the fin forces, while at higher speeds fin forces increase due to the direct impingement of the free stream.

The development history of the McDonnell Douglas AH-64 Apache also provides several examples of the potential importance of main rotor/tail rotor/empennage interaction. As Ref. 10 describes, the early versions of the AH-64 encountered significant trim excursions in forward flight and climb due to the unexpectedly large downwash of the main rotor wake on the T-tail horizontal stabilizer (Figure 2). Further complicating analysis and understanding of this phenomenon was the asymmetry of the downwash on the tail downstream of the main rotor (Figure 3). Lacking the tools to predict and analyze such wake-generated phenomena, extensive flight tests were required to diagnose and fix these problems. The AH-64 also encountered significant problems with unstable Dutch Roll motions due to the coupling of pitch motion with slideslip at high forward speed. Figure 4 illustrates the measured flowfield in the vicinity of the empennage showing the asymmetrical downwash that leads to the pitch/sideslip coupling in forward flight. Clearly, to capture inflow patterns like this accurately, an advanced wake model will be required.

The examples cited above are only a sample of the many interactional aerodynamic issues that are of interest for rotorcraft applications. Others include the determination of steady and unsteady loads on bluff structures like typical helicopter fuselages, and special effects due to the proximity of the ground. The problems discussed, though, emphasize the interaction of the main rotor wake with the tail rotor and lifting tail surfaces and are judged to be significant issues that may be addressed with technology that is currently available or may be developed from current analytical tools.

The problem as implied in the previous discussion is to calculate the steady and unsteady loads induced by the main rotor wake on fixed or rotating lifting surfaces downstream of the rotor. Previous work on the computation of

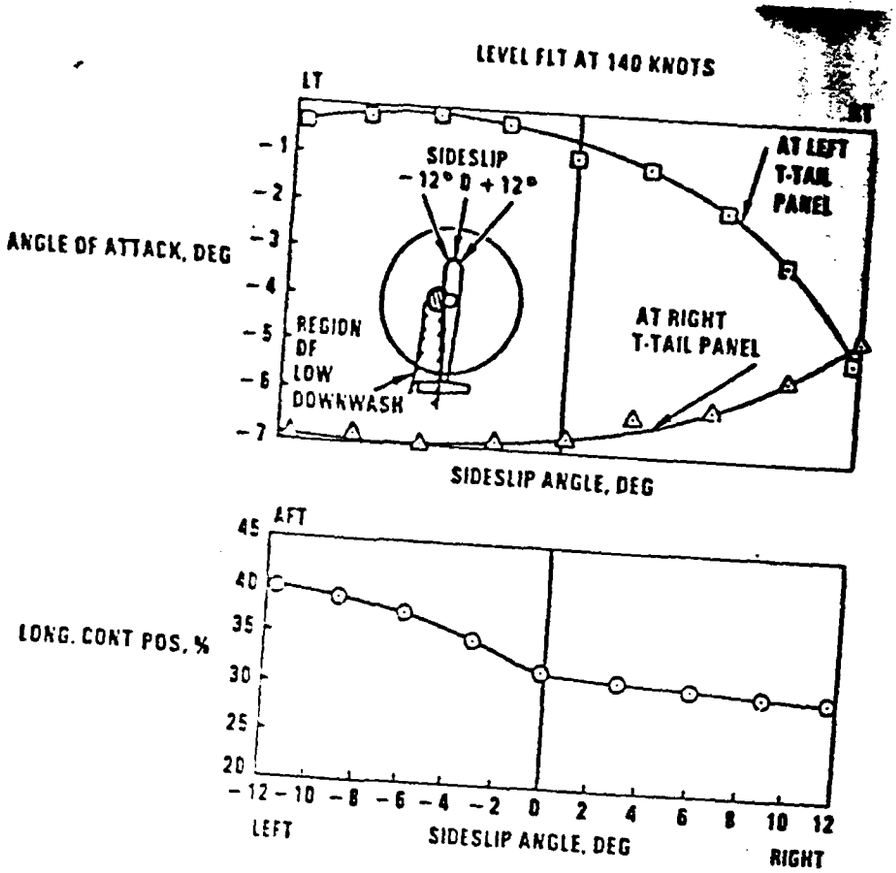

Figure 3. Downwash angle at tail and longitudinal stick required as a function of sideslip (Ref. 10).

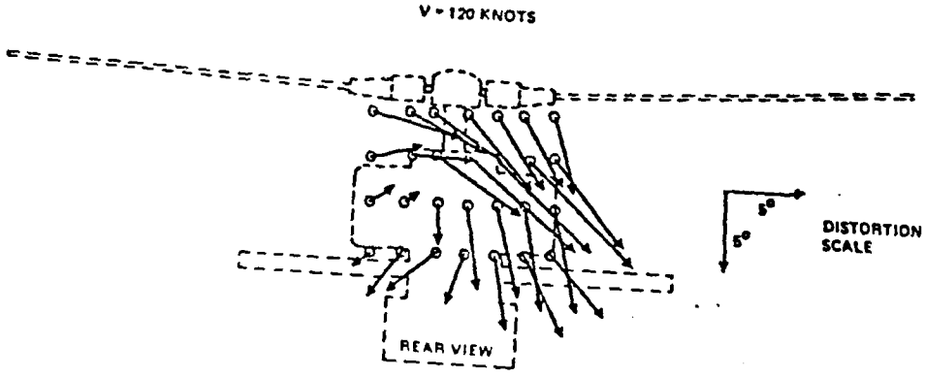

Figure 4. Experimental downwash/sidewash pattern in the wake of the AH-64 main rotor (tail rotor absent) (Ref. 10).

loads generated by vortex-dominated wakes of fixed-wing aircraft include an extensive literature on interactions of wings and isolated vortices. However, fewer efforts have been made to address to particular question of lifting surfaces in rotor wakes which feature complex interactions of large numbers of vortex filaments.

One attempt to address rotorcraft-oriented issues in this area is the work of Gangwani (Ref. 11). This work documents the development of a computational simulation of main rotor tip vortices interacting with fixed tail surfaces. The simulation described allows for the interaction of the individual tip filaments with a lifting surface representation of the horizontal or vertical stabilizers. However, the influence of vorticity trailed from the inboard portion of the blade is omitted, a questionable approximation given the strong bound circulation observed on the inboard regions of rotor blades in many regimes of practical interest. Also, Ref. 11 uses straight vortex elements to construct the distorted tip vortex filament. As discussed in Ref. 4, straight element approximations to highly distorted wake filaments can produce substantial errors in downwash velocity near the filament.

Recently, several other efforts have been undertaken that attack the problem of predicting interactional aerodynamic effects from a variety of view points. Egolf and Lorber (Ref. 12) coupled a prescribed rotor wake model to a doublet-based panel method to predict the unsteady surface pressures experienced by a simplified fuselage. Their analysis, however, assumed that vortex filaments followed the contours of fuselage surface and did not permit them to distort freely during the interaction. This nonphysical assumption raises serious doubts about the validity of the loads predicted. Rand (Ref. 13) carried out a similar analysis, again assuming prescribed vortex trajectories near the surface, and in this case using an even simpler wake model consisting of vortex rings. The results of Ref. 13 are thus subject to the same reservations noted for the work of Ref. 12.

Berry (Ref. 14) undertook an analysis which included a freely distorting vortex lattice model of the rotor wake. While this approach permits the wake geometry to adjust to the presence of the fuselage, it includes no special

treatment of the close interactions that take place between the vortex wake and the surface. Unless such interactions are carefully handled, large errors can be introduced, and this may account for the difficulty experienced in correlating measured loads in Ref. 14.

The recent work of Clark and Maskew (Ref. 15) features another treatment of a rotor wake model using sheet singularities in the presence of a paneled fuselage. This analysis features freely distorting quadrilateral doublet panels as well as treatment for close vortex-surface based on local increases in the panel density. The discussion below will indicate how the doublet panel method and the preconceptions about the wake vorticity field that it represents may be replaced by a more natural representation based on curved vortex filaments. Also, new methods for treating close vortex-surface interactions will be described that obviate the necessity for local repaneling of the surface.

1.2 Approach

The literature surveyed above shows both the significance of interactional aerodynamic effects and the broad similarity of the approaches taken to date to analyze interactional phenomena. The main body of this report describes the sigificantly different new departures that have been undertaken to study this problem and to provide the building blocks of a practical interactional aerodynamic analysis. The discussion of the Phase I results focuses on two of the most significant individual problems in the complex set of interdependent phenomena that goes by the name of interactional aerodynamics: first, the accurate prediction of wake-induced velocity fields of isolated rotors; and second, the development of physically valid and efficient models for vortex surface interactions. Success in these two endeavors does not by itself fill the need for a general interactional analysis implied by the experimental studies of rotor/wake and rotor/fuselage coupling described above. However, the basic assumption of this work is that given the ability to attack these two problems with confidence the foundations of such an analysis will have been established.

In the section below, a brief review of the basic rotor wake model used in this work will be presented. Following this, the major results of the studies of isolated rotor wakes using this model will be discussed. Finally, the new methods developed during this effort for the accurate and efficient simulation of close vortex-surface encounters will be described, and sample problems will be solved demonstrating the flexibility and robustness of these new methods.

2. PREDICTION OF MAIN ROTOR WAKE DYNAMICS

2.1 Review of Free Wake Analysis Techniques

Recently, considerable advances have been made in calculating the dynamics of complicated unsteady vorticity fields. As discussed in Refs. 4 and 5 application of the new vortex dynamics analysis method using curved vortex elements has lead to a dramatic improvement in the prediction of rotor blade higher harmonic airloading. In order to successfully predict rotor aerodynamic loads, it was found necessary to account for the vortex wake generated by the entire blade span, not just the tip region. Furthermore, the wake is modeled by a field of constant strength filaments which correspond to the actual resultant vorticity field in the wake. This natural representation of the wake is essential to the accurate prediction of the free motion of complex vorticity fields. This same approach has been found to be well suited for the development of an advanced methodology for rotorcraft interactional aerodynamics.

A theoretical and numerical analysis (Ref. 4) has shown that free wake flows involving close interactions between filaments should utilize curved vortex elements in order to guarantee a consistent level of accuracy. A similar conclusion applies for interactions with solid surfaces, such as occurs with problems in interactional aerodynamics. The curved element method was implemented into a forward flight free wake analysis and exhibited rapid convergence and robust behavior, even at relatively low advance ratio (Refs. 4 and 16). The full-span wake model using such Basic Curved Vortex Elements (BCVEs) has formed the foundation of the wake simulations used in Phase I.

At high advance ratio, the rotor wake structure is quite complicated and the simple tip vortex representation often used in the past is inadequate. On the advancing side, the generating blade may experience large spanwise and azimuthal load variations. The new wake analysis methods seek to represent the important features of the resulting wake generated along the full span of the blade.

Figure 5 shows the new full-span free wake generated by one blade of a four-bladed rotor at advance ratio 0.28. The particular analysis used in the Phase I effort was drawn from Ref. 5, which featured the implementation of a lifting surface model of the rotor blades to define the filament strengths in the freely interacting main rotor wake. It utilizes a numerical analysis based on the curved vortex described in Ref. 4. These elements are used to represent vortex filaments laid down along contours of constant sheet strength in the wake. The skewed/curved filaments provide a natural representation of the free wake vorticity field, which simultaneously accounts for both shed and trailed vorticity. An additional advantage of the method is that it provides a visually meaningful representation of the wake since the filaments correspond to the actual resultant vorticity field. The vortex filaments leaving the blade in Figure 5 are all of constant strength, and each one is of equal value. For this reason, close spacing between the filaments implies a strong net influence from that region of the wake, whereas a sparse spacing indicates a region having little effect.

An examination of Figure 5 shows that the advancing side wake is a complicated sheet-like structure, not a simple rolled-up tip vortex as has often been assumed. The looping (or connecting) between outboard and inboard filaments is associated with changes in the maximum bound circulation on the blade. A strong root vortex structure is also evident. The actual aerodynamic environment experienced by the following blades passing over this complex wake structure can also be seen in Figure 5. From the standpoint of aerodynamic interaction with downstream surfaces, this figure shows a remarkably complicated incident wake structure.

The preceeding discussion illustrates the one important feature of the approach used in Phase I; the ability to accurately represent the full-span rotor wake vorticity field. The discussion that follows will give examples of the success of this approach in generating accurate predictions of the velocity field downstream of the rotor. Also, this full description of the vorticity field is tracked by free wake methods as it interacts with the

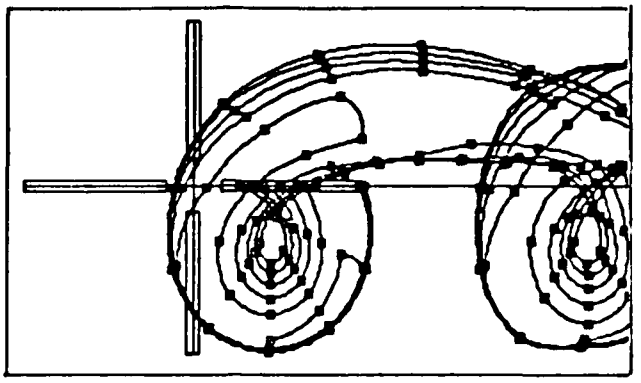

a) $\psi = 0°$

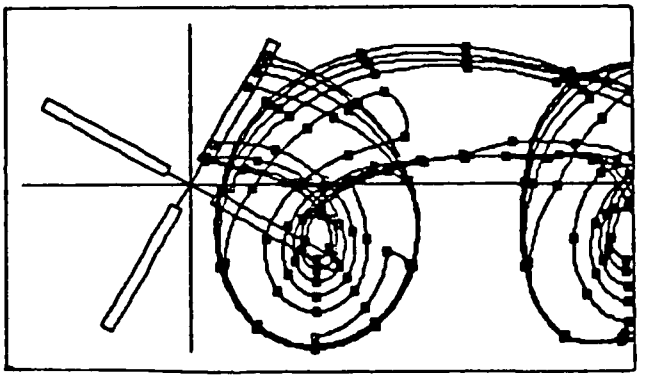

b) $\psi = 60°$

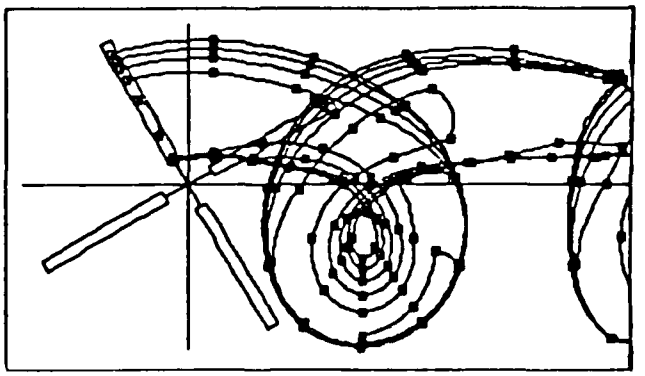

c) $\psi = 120°$

Figure 5. Wake geometry for the AH-64 main rotor at advance ratio 0.28. (Only one wake shown.)

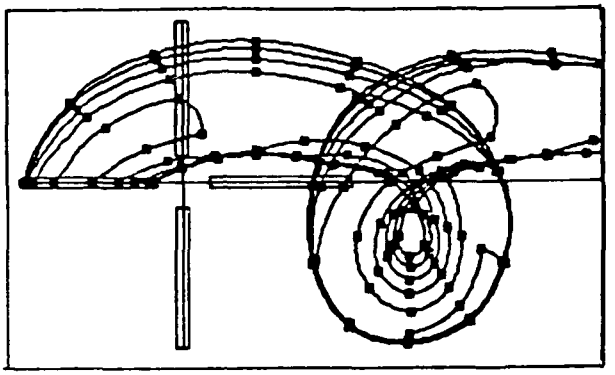

d) $\psi = 180°$

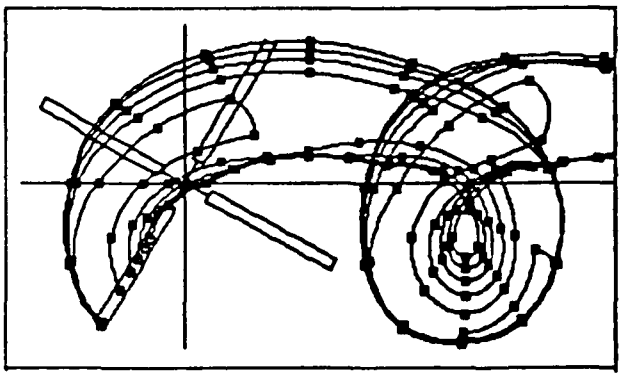

e) $\psi = 240°$

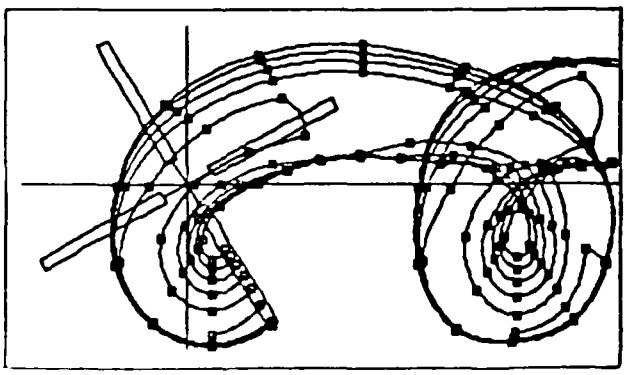

f) $\psi = 300°$

Figure 5. Multiple wake geometry for the AH-64 main rotor [illegible] ratio 0.28. (Only one wake shown.)

fuselage and lifting components, such as vertical and horizontal tail surfaces. Interaction with these solid surfaces may lead to rapid stretching and high distortion of the vortex filaments, and in some cases the filaments may split or be cut. Curved vortex elements are extremely well suited to represent vortex filaments under conditions of high stretching and distortion. However, additional research has been required to develop methods to effectively handle filaments in close proximity to boundaries and under conditions of extreme stretching and cutting. The work performed on this topic during the Phase I effort will be described later, in Section 3.

2.2 Prediction of Wake-Induced Velocity Fields

The portions of the helicopter downstream of the main rotor experience a wide variety of flow conditions throughout the flight envelope of typical rotorcraft. Given the range of advance ratios, sideslip and climb angles, and thrust coefficients of potential interest, it was not feasible during the Phase I effort to examine the full spectrum of possible wake flow configurations. Instead, several representative cases were chosen for close examination, two of which are discussed here. First, wind tunnel tests of an isolated main rotor at moderate advance ratio of 0.14 (from Ref. 17), and second, tests of an AH-64 scale model at high forward speed (from Ref. 18). The flow fields generated in these tests contain many phenomena of interest in interactional aerodynamics and, thus, the results of these simulations represent meaningful tests of the suitability of the free wake methods described above for this effort.

The results of Ref. 17 include velocity measurements in crossflow planes at several stations downstream of the rotor. Figure 6a shows a comparison of the measured and computed crossflow velocities in a plane 1.07R downstream of the rotor hub at advance ratio 0.14. The dominant feature of both the computations and experiments is the strong swirling flow trailing from each edge of the rotor disk; these well-known features represent the rolling-up tip vortices that are evident in the visualization of this case in Figure 6b. This figure shows not only the strongly concentrated tip vortices but also the

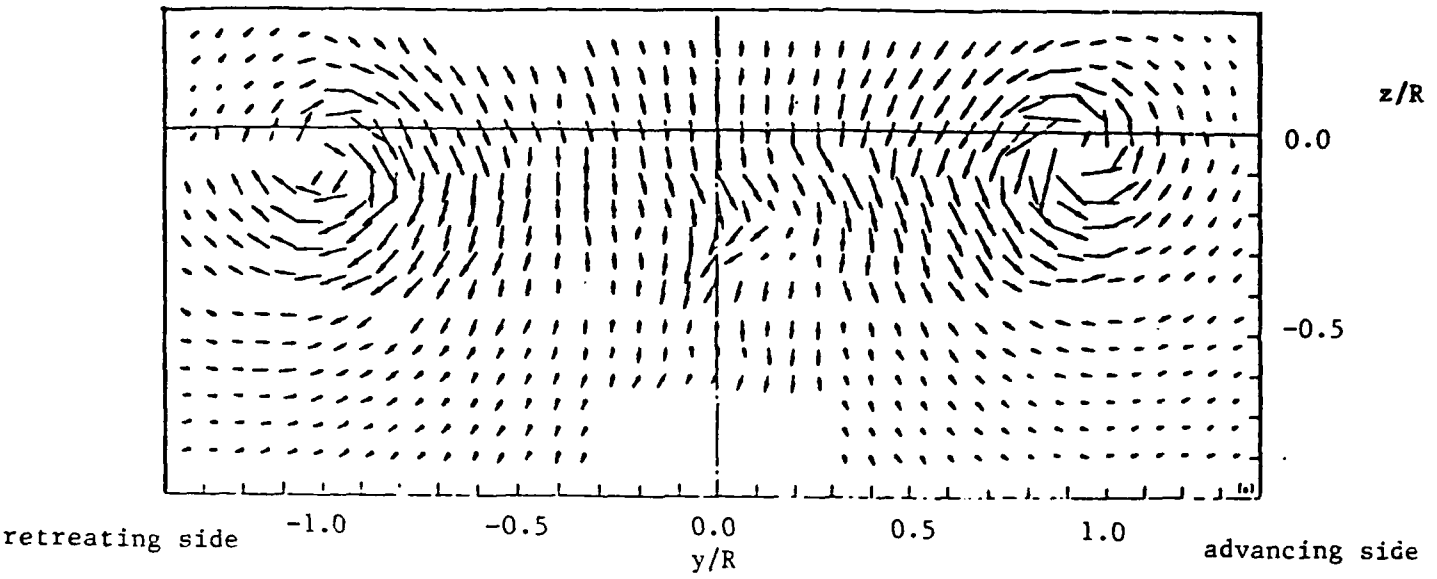

Figure 6a. Crossflow velocity plot 1.07R downstream of main rotor hub (from Heyson). Advance ratio = 0.14 , tip speed = 500 fps , R = 7.5 ft .

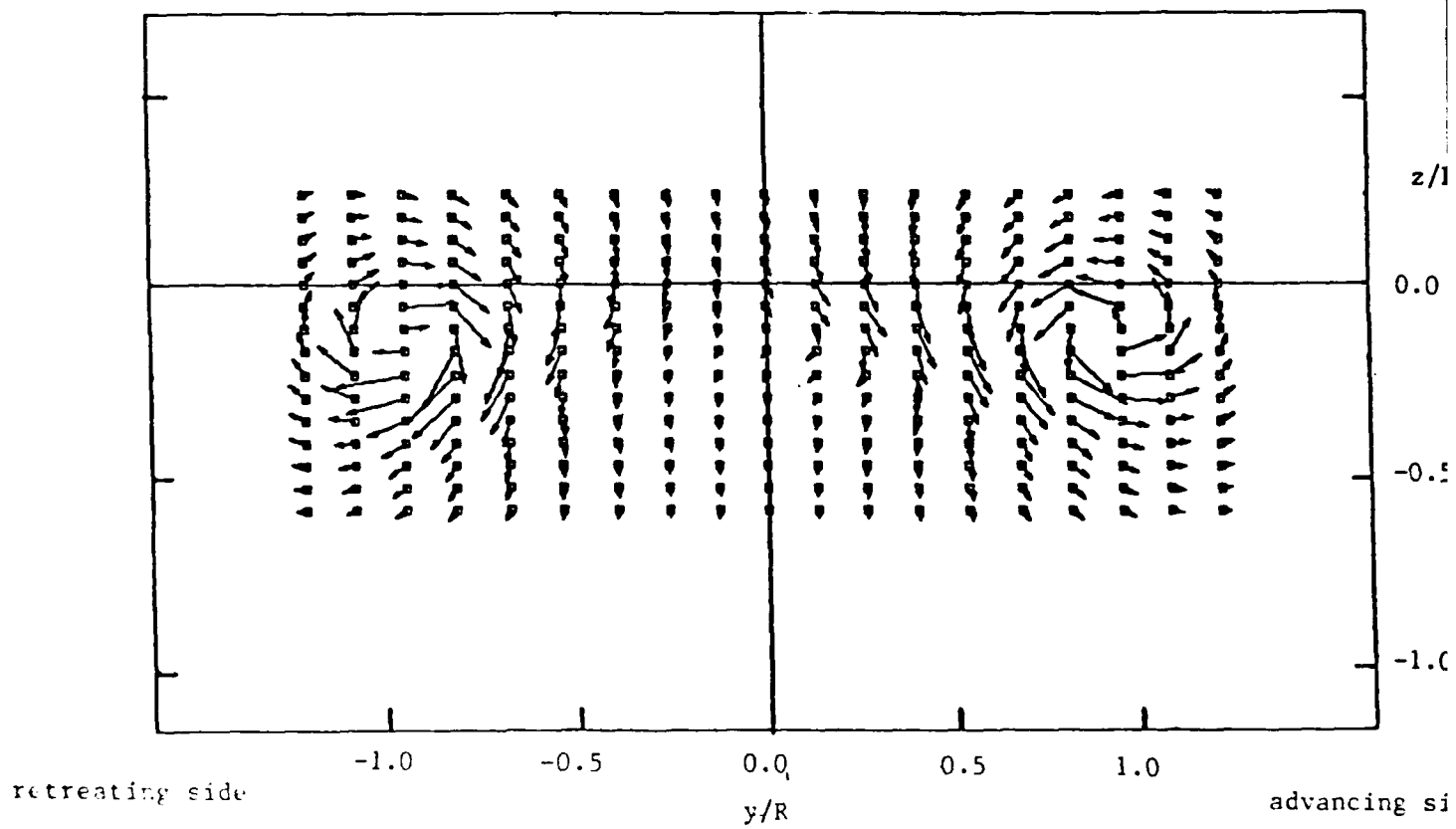

Figure 6b. Prediction of the above data using a ten-filament model.

complex structure of the trailing wake from the inboard portions of the blade. It is this portion of the wake that bring about such features as the very noticeable crossflow on the advancing side at $z/R = -0.3$ and $y/R = 0.2 - 0.4$. Even this feature is captured in the computational crossflow plot of Figure 6b which shows the results of a simulation using ten filaments on the span. Therefore, even though the computational results do not duplicate every feature of the measured flow (note too, that both plots in Figure 6 are to the same scale in both position and velocity) the correlation achieved is very favorable.

The same set of experimental results are examined in more detail in Figures 7 through 9. Here distributions of downwash are shown for three-vertical stations: 0.17R above the disk, as well as 0.17R and 0.33R below the disk in Figures 7, 8 and 9, respectively. Again, all of these surveys were taken at 1.07R downstream of the rotor. In each of these figures, the data are compared with the computed downwash from three different wake models: a two-filament model (i.e., just root and tip vortices at each azimuth), as well as models with six and ten filaments on the span. These results show the trend in the predictions as the wake model is refined.

Beginning with Figure 7, note that the two-filament model considerably overpredicts the measured data, whereas the more refined models, while underpredicting the results somewhat, are noticeably closer. (Note: the jaggedness in the data is due to digitization from the original plotted results; also, the stated experimental error here is ±10%.) In Figure 8, both the computations and the data considerably reflect greater spanwise variation, due to the proximity of the measurement points to the rolling-up wake. The difference between the predicted results of the two-filament model and the more refined computational results is much more pronounced. The relatively refined six- and ten-filament models capture the peak downflows well on the advancing side, and the trend on the retreating peak is clearly toward the experimental result as the model is refined. Near the center of the wake, the model once again underpredicts the data, although again the favorable trend is clear as the wake is refined. Similar results are evident in Figure 9, which details the downwash distribution still farther down in the wake. The same pattern of improving correlation with the refinement of the model appears.

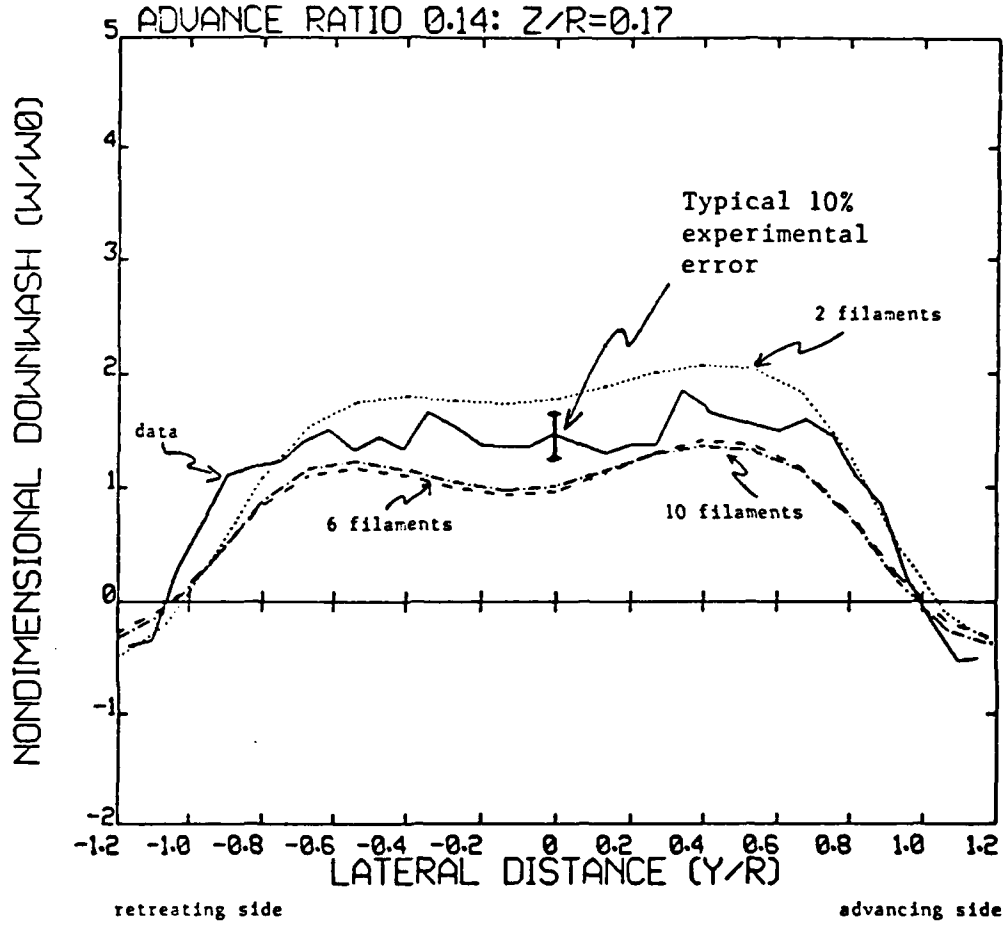

Figure 7. Nondimensional downwash at various lateral positions 1.07R downstream of the hub of a two-bladed rotor. (Wind tunnel tests at advance ratio 0.14, C_T = 0.0037 .) Vertical station 0.17R above the rotor disk.

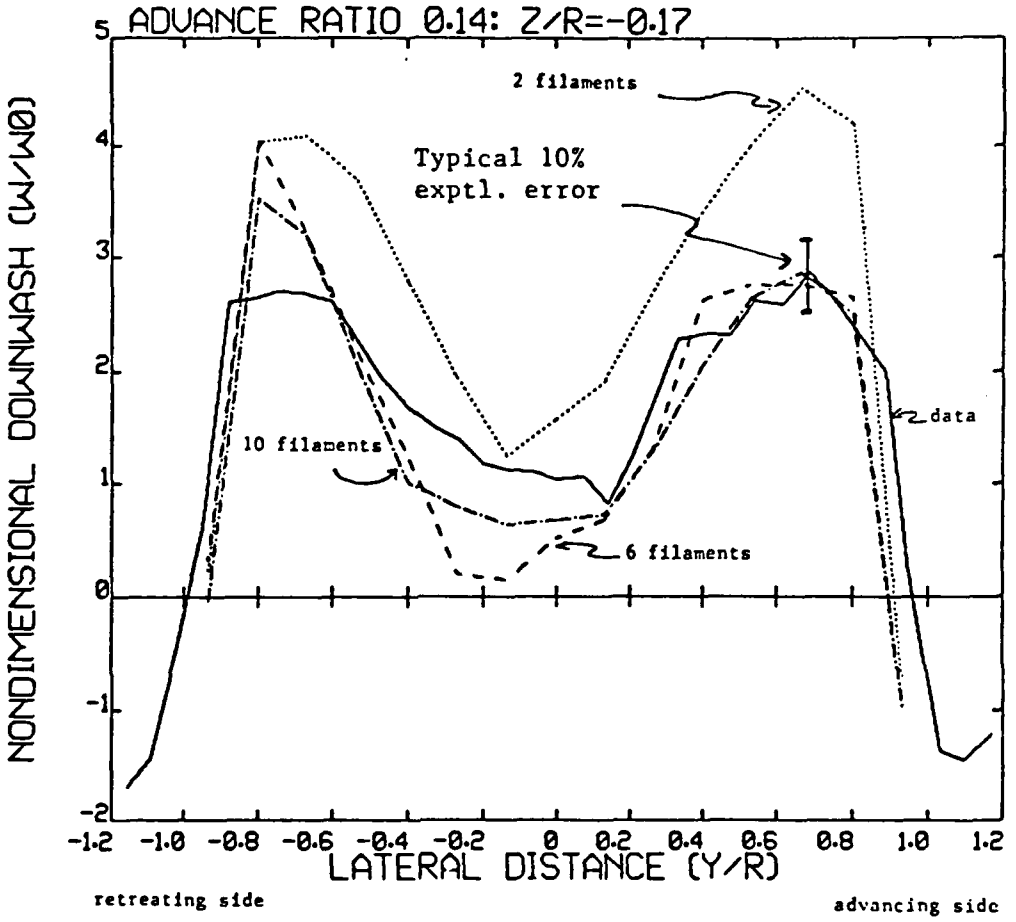

Figure 8. Nondimensional downwash at various lateral positions 1.07R downstream of the hub of a two-bladed rotor. (Wind tunnel tests at advance ratio 0.14, C_T = 0.0037 .) Vertical station 0.17R below the rotor disk.

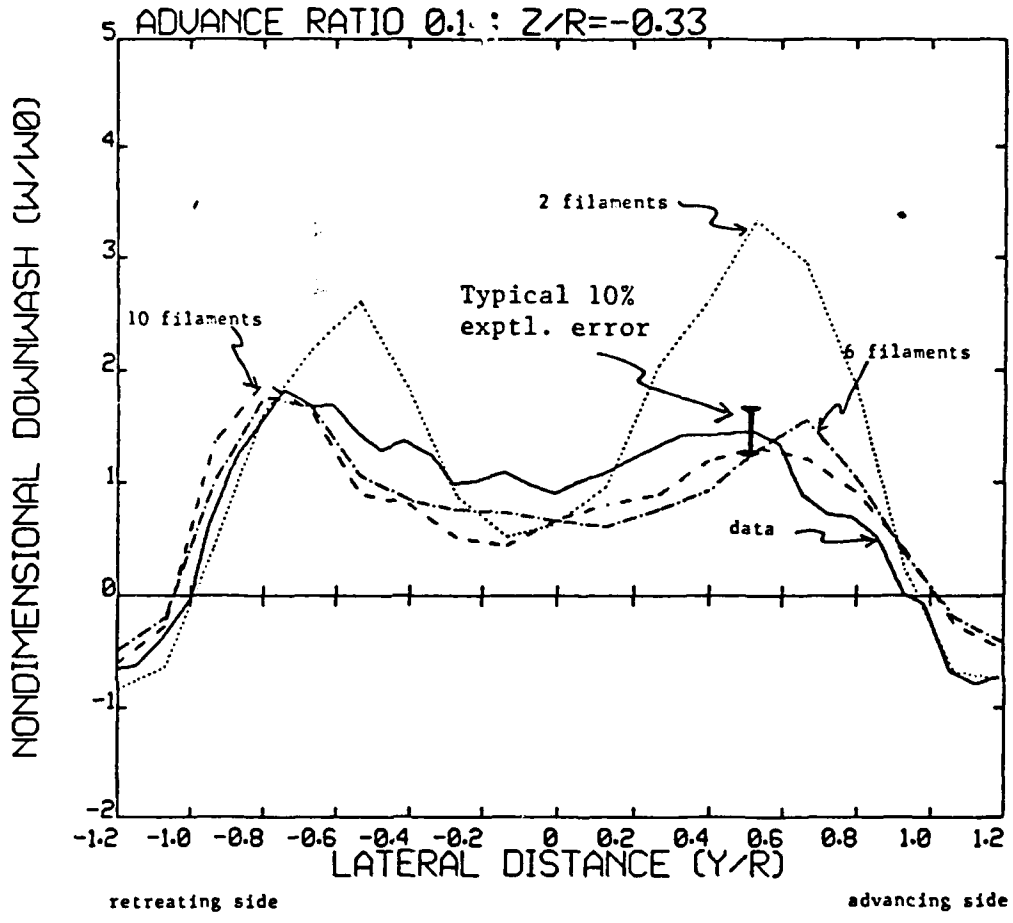

Figure 9. Nondimensional downwash at various lateral positions 1.07R downstream of the hub of a two-bladed rotor. (Wind tunnel tests at advance ration 0.14, C_T = 0.0037 .) Vertical station 0.33R below the rotor disk.

Along with these low-speed computations, simulations of the high speed model tests reported in Ref. 18 were undertaken. These tests focused on measurements of the flow downstream of the main rotor of an 0.30-scale model of an AH-64 at a tunnel speed of 204 fps (advance ratio 0.28 for a full-scale AH-64). In this flight condition, the characteristic crossflow pattern is markedly different than the low-speed results discussed above. The experimental results shown in Figure 10 indicate the presence of a strong swirling flow in the vicinity of the tail of the helicopter. (The "waterlines" in Figure 10 refer to vertical reference heights in the experiment.) A recent survey paper on the relation of aerodynamics to handling qualities of rotorcraft (Ref. 19) cast doubt on the ability of even sophisticated computational analyses to capture the type of results shown in Figure 10. The good qualitative correlation displayed in Figure 11 is, thus, particularly noteworthy. The results shown there reflect only the wake-induced velocities, with no accounting for the wakes of the rotor hub or the fuselage. In spite of this, it is clear that most of the major features of the flow in Figure 10 have been captured, and that, by inference, the rotor wake exerts a dominant influence on the flow near the tail.

The computational results of Figure 11 used a relatively simple six-filament model. The value of adding even such a coarse treatment of the inboard wake is evident from Figure 12, which shows the inflow predicted on the same grid of points with only a tip filament present. It is of interest, as well, to examine the details of the correlation achieved with this type of wake model. Figure 13 shows the predicted and measured downwash distributions at four vertical stations ("waterlines") within the measurement grid of Figure 10 using both two- and ten-filament models. Although some details do not agree, the overall pattern of good correlation is clear. The correlation on the advancing side improves noticeably as the wake is refined, while some errors persist downstream at the reverse flow region. Note in particular the asymmetry of downwash, a well-known feature whose origin will be discussed in the next section.

The prediction of the sidewash components in the wake was found to be a more difficult undertaking. As shown in Figure 14, even with the rotor blades

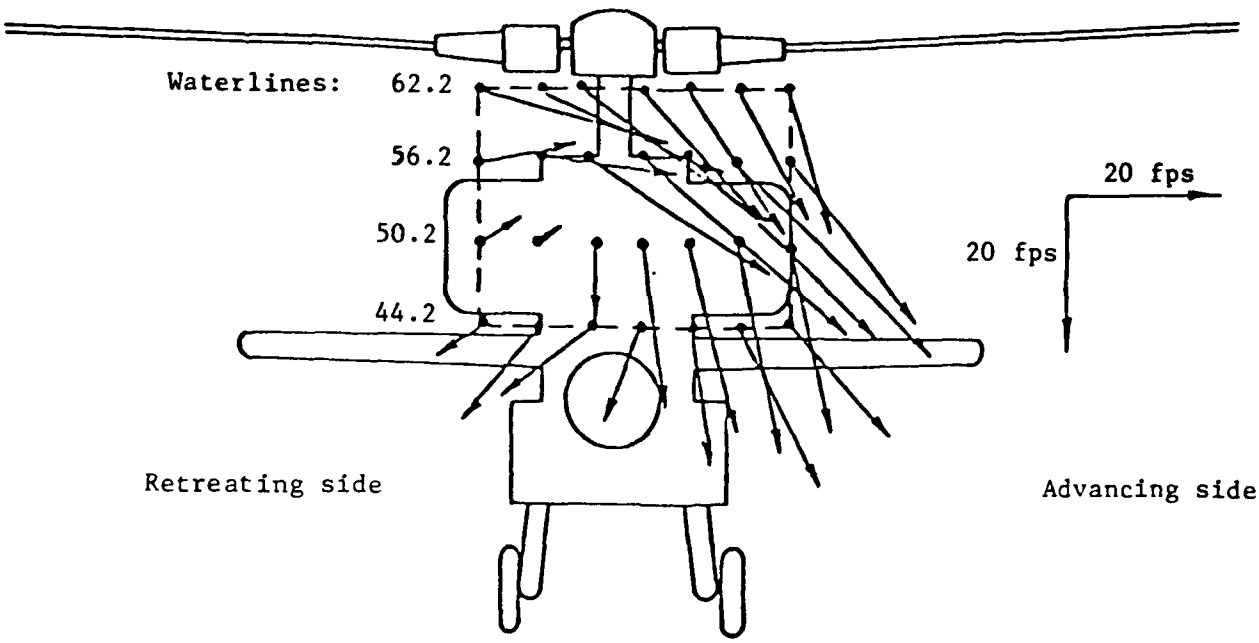

Figure 10. Crossflow velocities for AH-64 wind tunnel model, 1.3R downstream of main rotor hub. Advance ratio = 0.28. Fuselage present, no tail rotor (from Ref. 18).

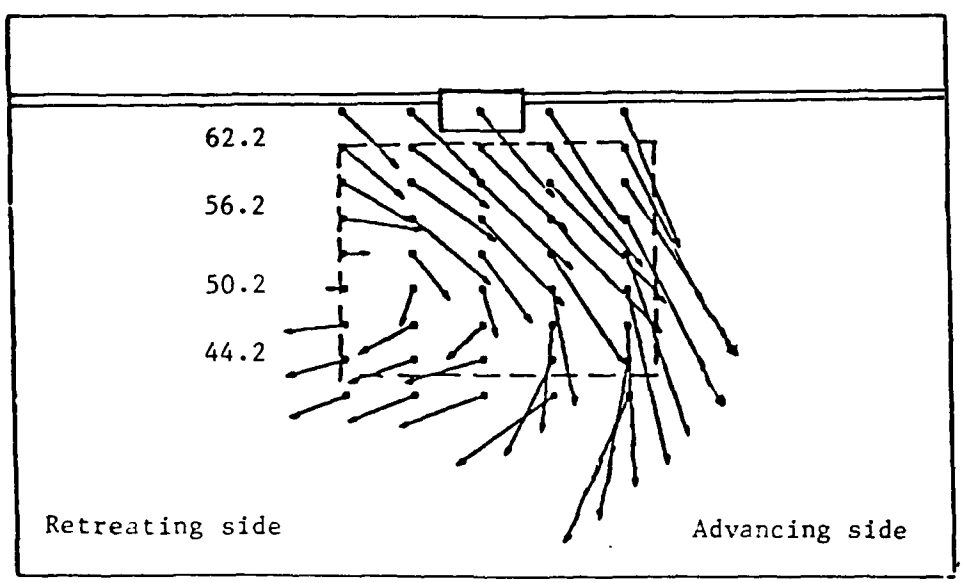

Figure 11. Prediction of AH-64 crossflow data. Velocity and distance scale identical to data. (AH-64 main rotor is 24.0 ft.)

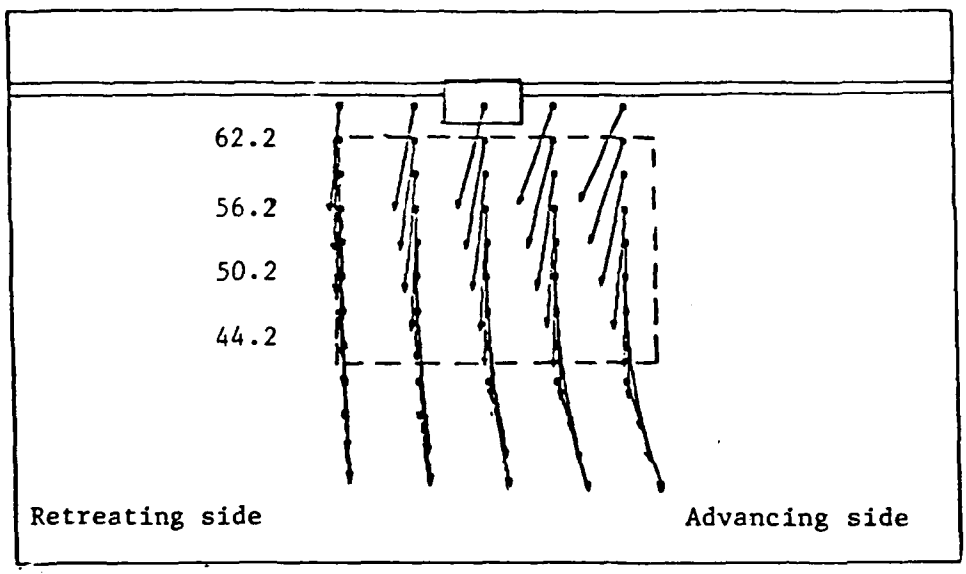

Figure 12. Prediction of AH-64 crossflow with tip vortex flow field only .

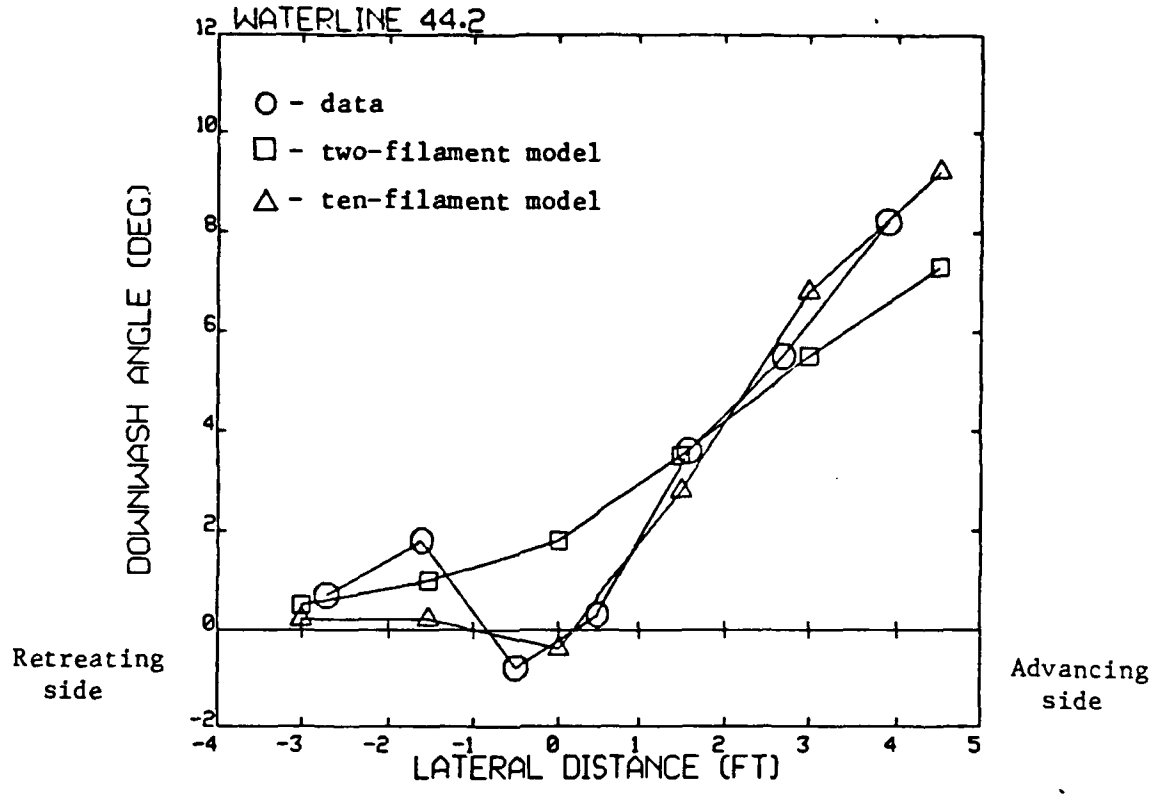

a) Waterline 44.2

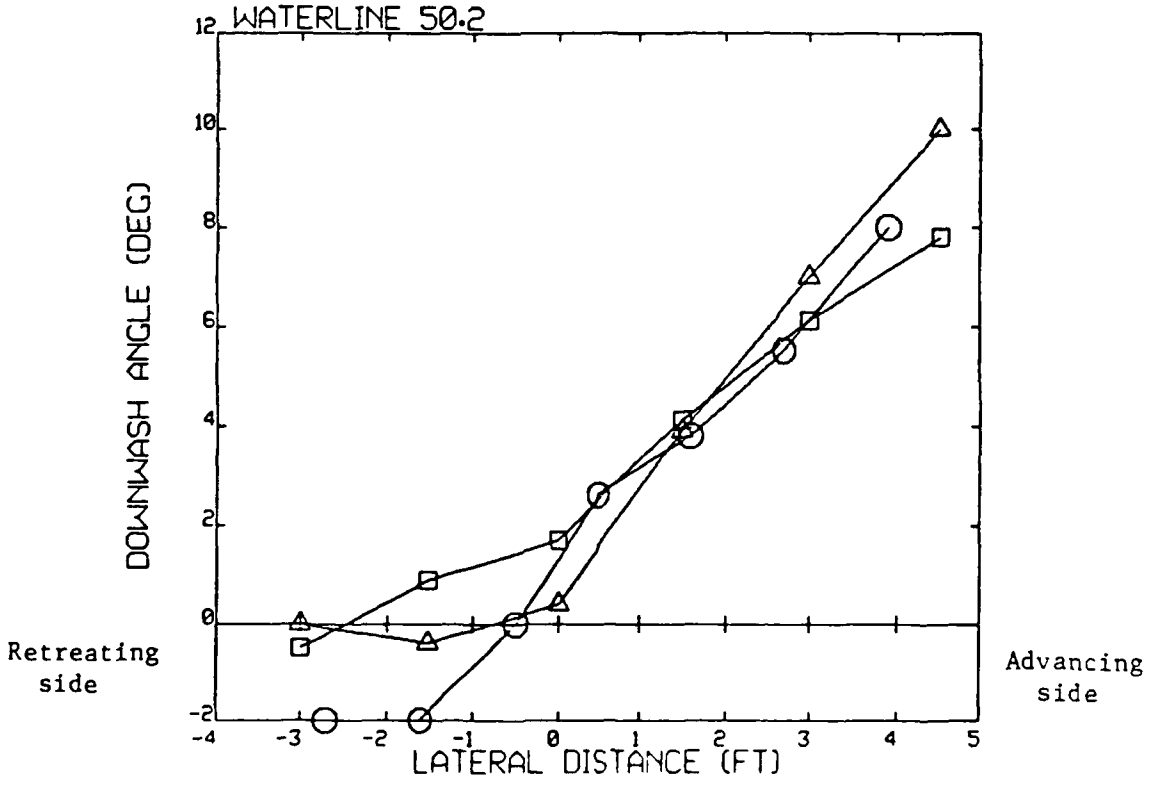

b) Waterline 50.2

Figure 13. Downwash angles at various lateral stations located 1.5% downstream of AH-64 model rotor. (Note: R = 24.0 ft.)

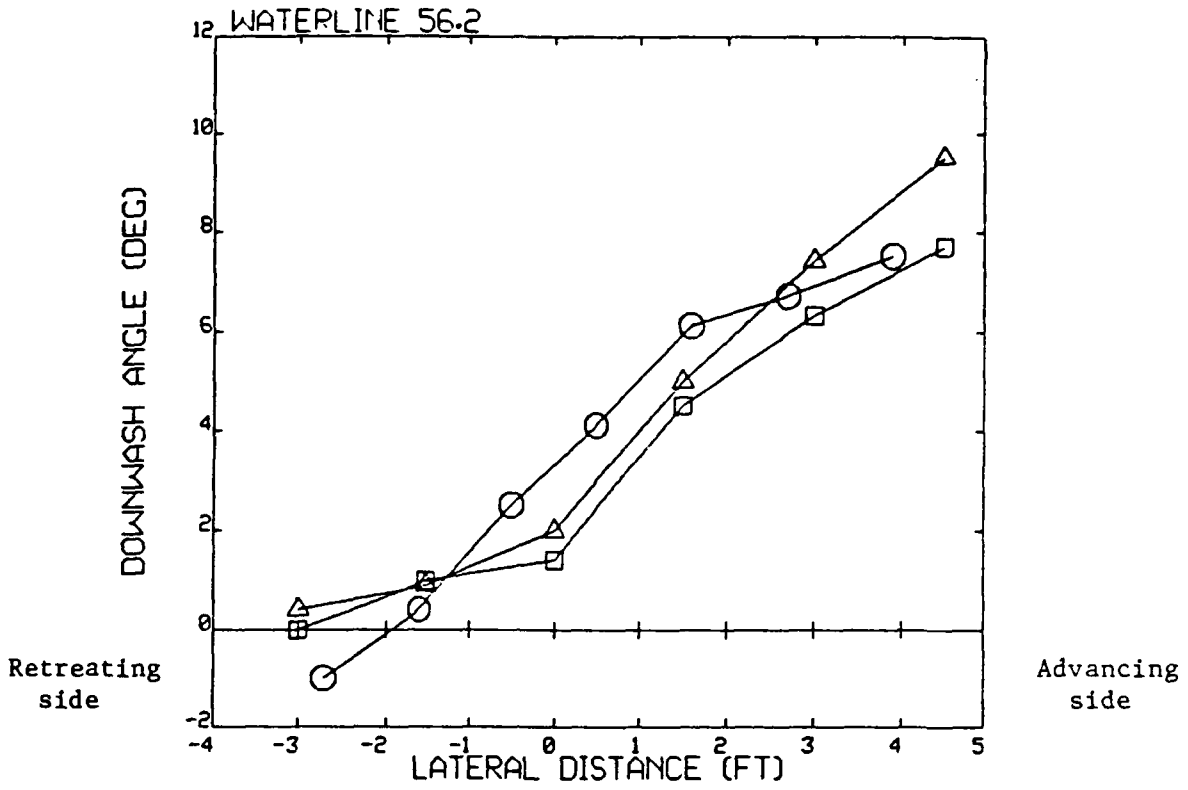

c) Waterline 56.2

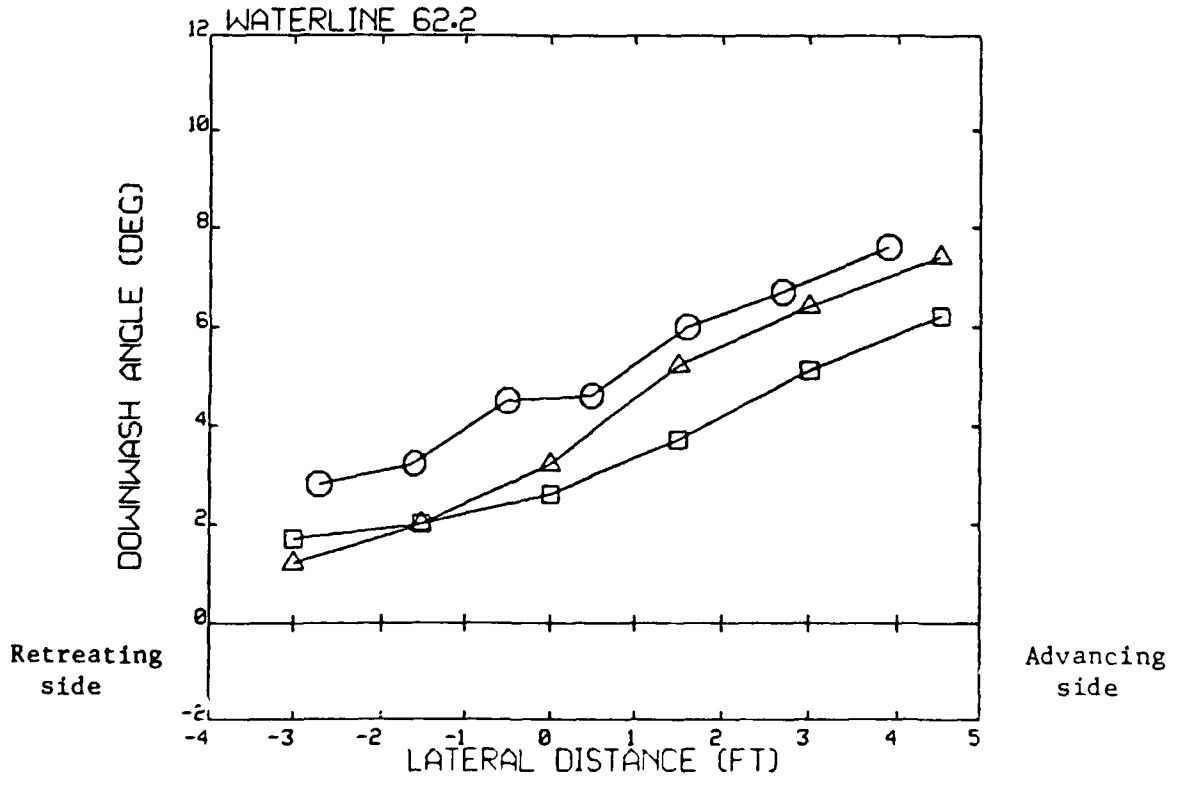

d) Waterline 62.2

Figure 13 (Cont'd). Downwash angles at various lateral stations located 1.2R downstream of AH-64 model rotor. (Note: R = 24 ft.)

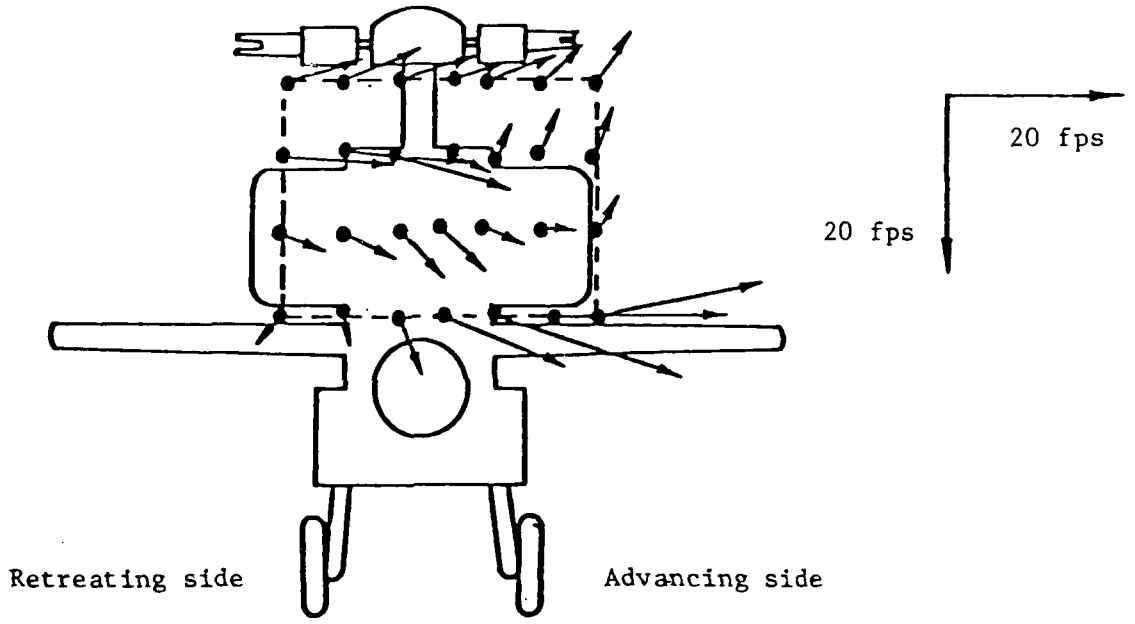

Figure 14. Crossflow distribution with rotor blades off, AH-64 model at advance ratio 0.28 (from Ref. 18).

removed, substantial velocities are generated by the hub and fuselage wakes. Since these velocities are principally sidewash, the downwash predictions of the rotor-only computations shown in Figure 11 are not greatly affected (although the small residual downwash angles were subtracted from the velocity vectors in Figure 10 before Figure 13 was plotted). The predicted rotor sidewash profile is shown in Figure 15. The characteristic vertical sidewash gradient suggests the presence of a vortex sheet of varying strength near the center of the computational grid. (The source of this feature will be discussed below, as will its implications for helicopter trim and flight dynamics.) It is evident, however, from the inspection of Figure 14 that the current wake-only model cannot capture the experimentally observed sidewash velocities. Clearly, the successful prediction of sidewash components will require the inclusion of the effects of nonlifting components (such as the rotor hub) in subsequent work.

2.3 Identification of Major Interactional Mechanisms

As is clear from the literature on experimental studies of interactional aerodynamics (e.g., Refs. 6-10), the range of possible interactional mechanisms in rotorcraft is extremely wide, encompassing interactions between the main rotor and the empennage/tail, the main rotor and the ground, the hub and the empennage, to name just a few. The focus of the Phase I feasibility study was on the first class of mechanisms listed above, since it was judged that the tools available were best suited to address such mechanisms and that they represented particularly significant phenomena. The results of the simulations discussed in the previous section can be used to identify the major rotor/tail interactional mechanisms in forward flight.

In low-speed forward flight at zero sideslip the velocity field induced by the main rotor in the vicinity of the tail is predominantly a downwash, as is evident from Figures 6 - 9. This downwash is generated by the rolling-up vortices on either side of the wake, while the tail sits in a region relatively free of direct impingement of such rolled-up vortices. The principal challenge for an interactional aerodynamics analysis in such flight

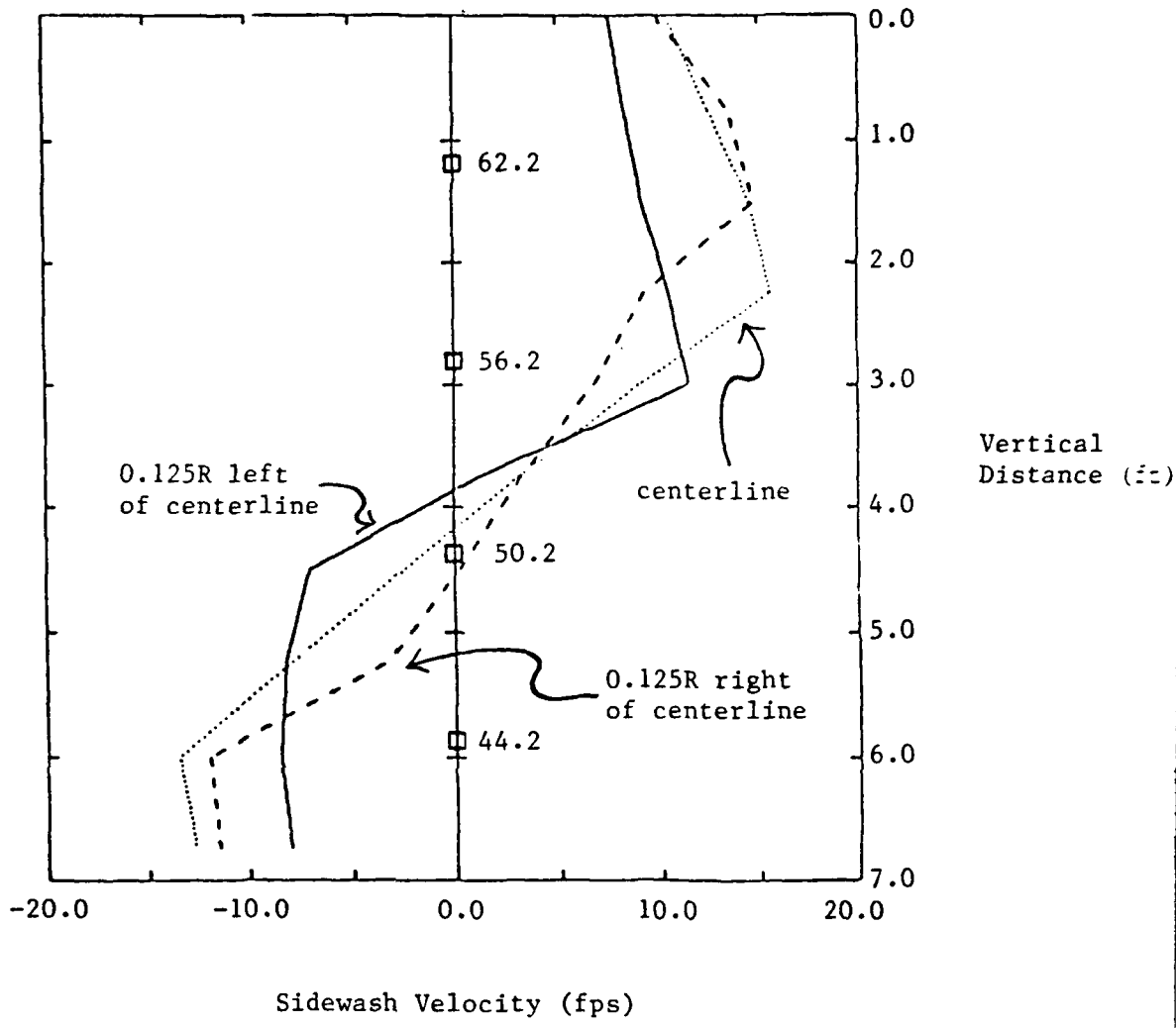

Figure 15. Sidewash distributions for the AH-64 at advance ratio = 0.28 , 1.3R aft of main rotor hub. Velocity is positive to the right looking from the rear. Vertical distance is positive down. (R = 24.0 on full-scale AH-64.) Boxes indicate vertical reference waterlines.

conditions is to predict the level of downwash on the tail as a function of forward speed and climb rate. Flight tests (Ref. 10) have shown a strong sensitivity of fuselage attitude to wake-induced downwash on horizontal stabilizers in low-speed flight as well as rapid changes in trim for climbing and descending flight. The good correlation demonstrated in the previous section is promising evidence of the ability of the wake model developed in Phase I to predict such effects.

In low-speed flight with sideslip, the possibility arises of the impingement of the rolling-up wake on the vertical stabilizer and the tail rotor. The strength and highly concentrated nature of these rolling-up vortices in low-speed flight is evident from the visualization in Figure 16. The experimental studies of Ref. 9 on wind tunnel models of an OH-58 aircraft make clear the potential importance of such wake-induced loads on the aircraft yaw moment and, thus, on lateral/directional trim in sideslipped flight or in hover in crosswind. The correct prediction of such loads is the topic of the next section, which discusses main rotor/tail rotor interaction.

In flight at higher forward speeds, the fundamental nature of the wake-induced flow in the vicinity of the tail changes dramatically, as seen in Figure 10. In such flight conditions, the flow develops strong gradients in both downwash and sidewash, gradients which have largely been unrecognized or treated in an approximate fashion in previous analytical work on helicopter trim and low-frequency flight dynamics. The origin of these gradients lies in the evolution of the wake into a nearly flat, sheet-like structure at high speed. This circumstance is reflected in the side view of the computed wake trajectory at advance ratio 0.28 in Figure 17, as well in the sidewash gradients seen in Figure 15. This computational result parallels the analytical finding of Ref. 20 which indicated that the wake of the rotor aft of the disk in high-speed flight could be well represented by a sheet of vorticity with vortex lines wholly parallel to the direction of flight. The origin of the lateral gradient of downwash, noted above, lies in the structure of this sheet-like wake; the cancellation of the "loops" of trailing filaments on the retreating side in Figure 17 and the reinforcement of the stretched filaments parallel to the free stream velocity yield a downwash distribution of the type seen in Figure 13.

Top View

Side View
(expanded
vertical
scale)

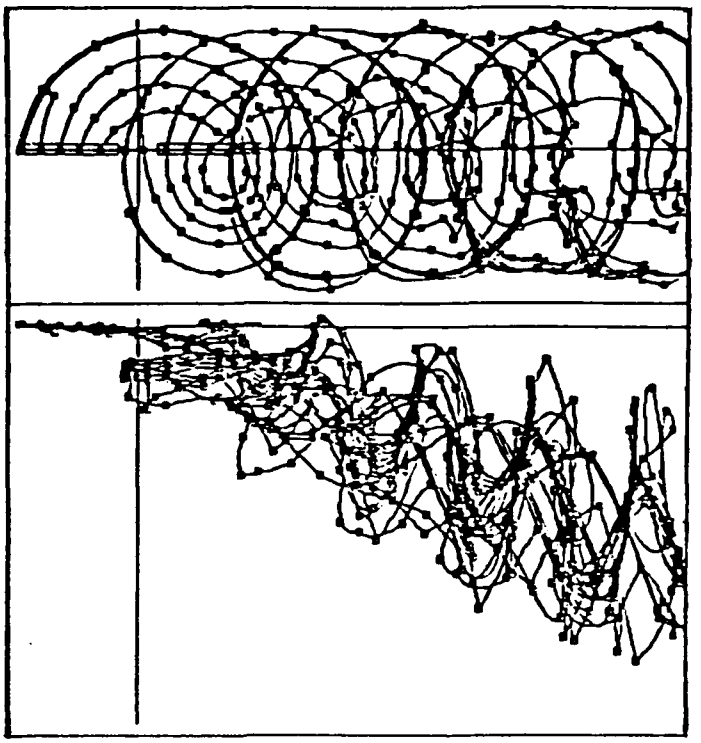

Figure 16a. Wake geometry for a two-bladed rotor at advance ratio 0.14, C_T=.0037: wake of one blade.

Top View

Side View

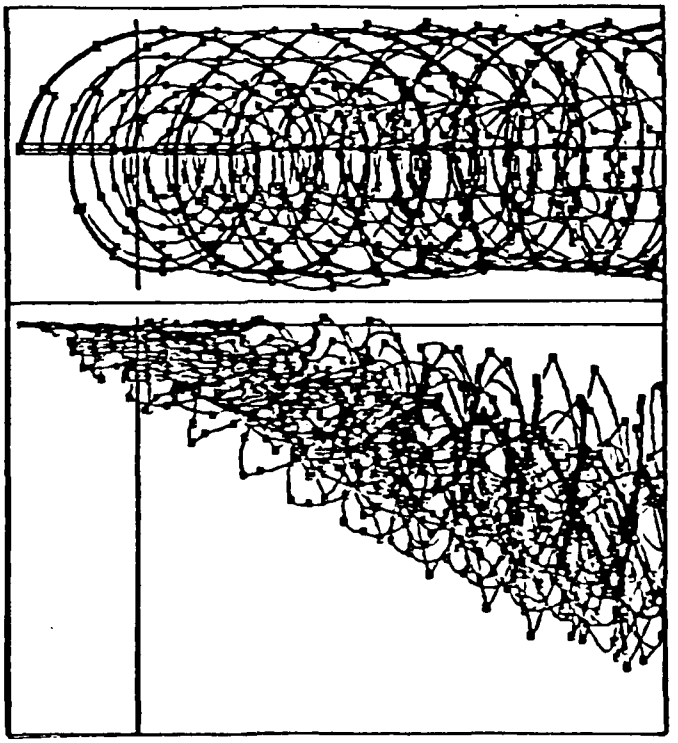

Figure 16b. Wake of both blades for the same flight condition.

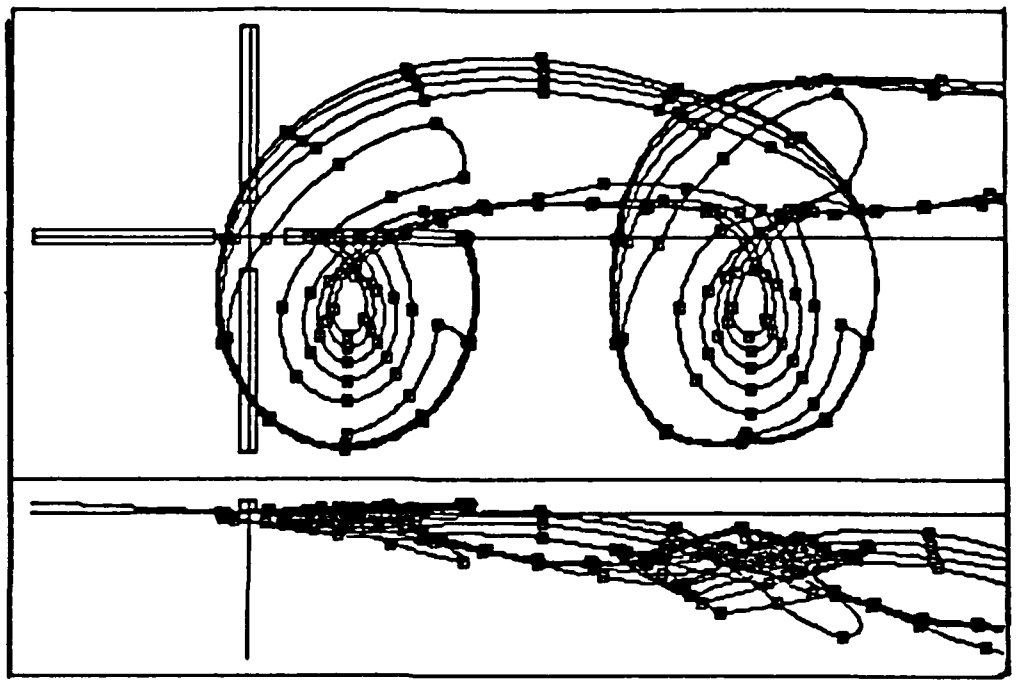

Figure 17. Top and side views of wake geometry for AH-64 main rotor at advance ratio 0.28; wake of one blade at $\psi = 0°$. Wakes of the other blades are present in the calculation but not illustrated. (Side view expanded by 2.0 in vertical dimensions.)

The potential significance of this type of interaction is considerable, in that the velocity field experienced by the tail rotor and vertical stabilizer will vary dramatically during any yawing or pitching motions of the fuselage. Moreover, the sign of the sidewash gradient in Figure 15 is such as to amplify the yawing motions of the fuselage in high-speed flight. This may help account for the light damping of the Dutch Roll mode experienced by several helicopters (see, for example, Ref. 10) in high-speed flight. Attempts to predict the details of fuselage response in high-speed flight in the presence of the rotor wake are hampered by the absence of a model for the sidewash generated by the hub and fuselage in the current simulation. Developing such a model is one of the likely technical objectives of future work on this topic.

2.4 Prediction of Main Rotor/Tail Rotor Interaction

Another component of considerable potential importance in interactional aerodynamics is the tail rotor. Experimental work to date (e.g., Refs. 6 and 9) has identified a variety of significant interactions involving the tail rotor, including main rotor/tail rotor and tail rotor/vertical fin. Given the absence of a model for the fuselage or empennage, only the former was examined during the Phase I effort. It was judged to be of interest to investigate the ability of a relatively simple model of the tail rotor and its wake to predict experimental data on tail rotor thrust in the presence of the main rotor. Reference 9 is one source for such data; it documents tests of an OH-58 main rotor operating with a scale model tail rotor in forward flight. The data chosen for correlation in this preliminary effort was a sweep of aircraft yaw angles (i.e., the inclination of the line between the main rotor hub and the tail rotor hub, to the free stream, in the absence of a fuselage) at advance ratio 0.11.

The tail rotor model used for this comparison consisted of a blade element model for the calculation of rotor loads coupled to a simplified representation of the tail rotor wake as a skewed cylinder of vortex rings. Figure 18 shows a schematic of the model. The spacing and orientation of the wake was determined by the free stream and the induced velocity at the

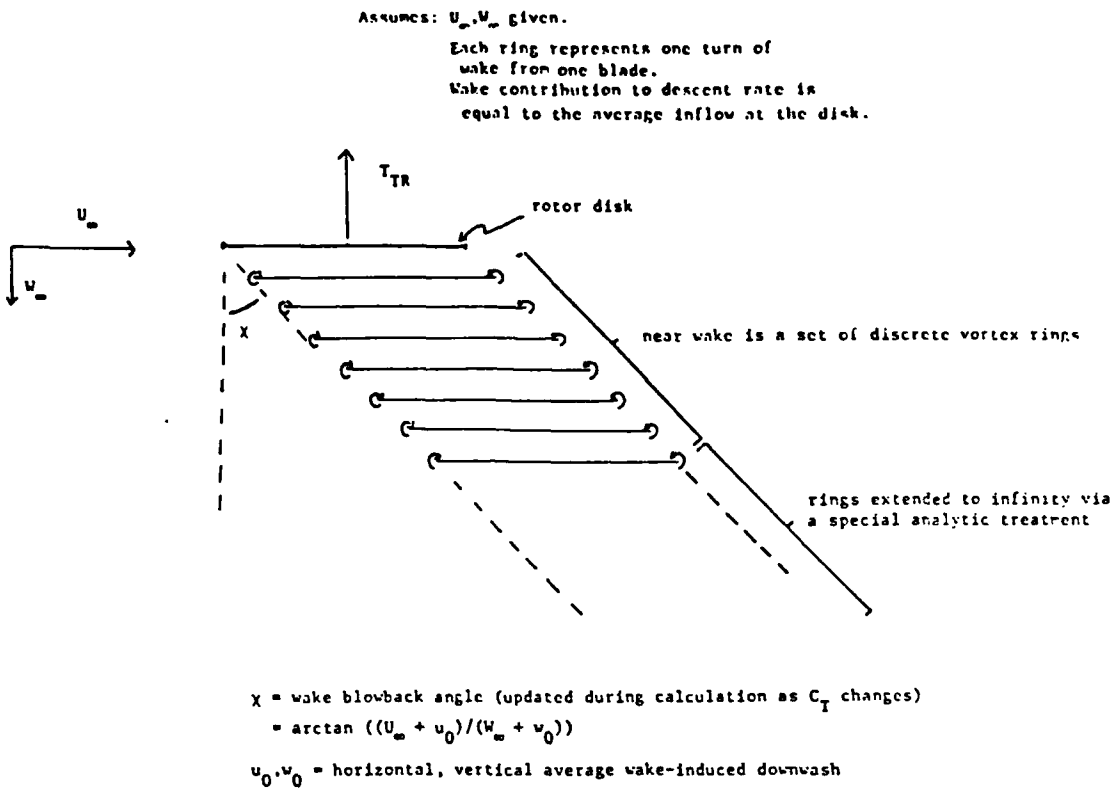

Figure 18. Schematic of prescribed wake model for the tail rotor.

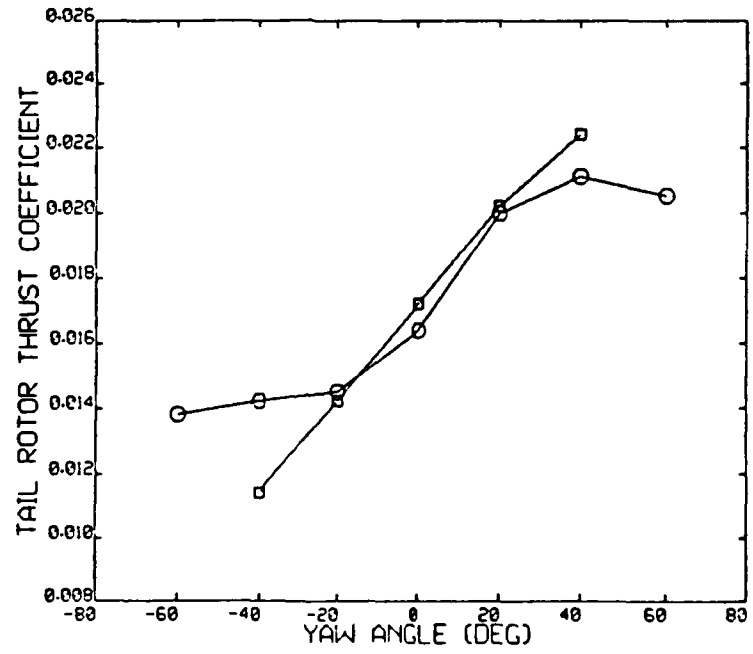

Figure 19. Prediction of tail rotor thrust at various yaw angles for OH-58 model rotor at advance ratio 0.11, $C_T = 0.0023$. Tail rotor collective fixed at 19°. (Circles = data; squares = predictions.)

tail rotor disk; the latter was updated as the calculation progressed. Given the tail rotor geometry and the pitch setting, the tail rotor average thrust could be computed.

Figure 19 shows the results achieved for a sweep of yaw angles between ±40°. For these cases, the main rotor thrust coefficient was 0.0023, and the tail rotor collective was 19°. Figure 19 indicates that near zero yaw angle, the thrust is reasonably well predicted using this simple model. However, as the yaw angle goes to ±40°, substantial errors are made as the rolling-up main rotor vortices impinge directly on the tail rotor disk.

3. NEW METHODS FOR VORTEX/SURFACE INTERACTIONS

3.1 Problem Statement

A major problem in the use of a vortex filament free wake analysis for interactional aerodynamics is the treatment of those filaments interacting with solid bodies. This problem has received very little careful attention in previous research. Neglecting the effect of the body on the wake, and using the wake to define a local incident flow is the simplest approach at present. However, this neglects the complex interactions and distortions that actually occur as the wake encounters the body. On the other hand, prescribing the filament motions in the presence of the body, e.g., as in Ref. 12, leads to violation of basic laws of vortex dynamics. In this case, prescribing the positions effectively creates bound vortices and these produce a Kutta-Joukowski force. Applying the momentum theorem to a control volume around the body and these vortices then shows that the force on the body is incorrect if forces are also being applied to vortices that should be free. It can be concluded that only by being faithful to the physics of the problem will reliable engineering solutions to the interactional aerodynamics problem be obtained.

The present approach is directed toward simulating the physically correct free motion of vortex filaments in proximity to bodies and aerodynamic surfaces. In the current work, the free wake is comprised of resultant constant strength vortex filaments which form an inherently natural representation of the vorticity field. This approach allows for a more physically correct and accurate analysis of wake dynamics than is obtained by lattice or panel wake representations which use vorticity components rather than the resultant filament strength and orientation. This distinction is particularly important in regions of high wake distortion, such as occur in wake body interactions.

The use of a physically realistic wake representation allows the development of wake/body interaction methods based on fundamental vortex

dynamics principles. Furthermore, this approach facilitates the use of local solutions to accurately treat close proximity filament interactions with bodies and surfaces. A central feature of the proposed effort is the use of local solutions, obtained either analytically or numerically, matched into the overall flow field.

3.2 Vortex/Surface Interactions

Vortex interactions can be categorized into two types: smooth body interactions and cutting interactions. In the case of smooth body interactions, the filaments approach a body surface in a roughly parallel manner. An example is rotor tip vortex filaments being blown down onto a fuselage top surface. On the other hand, cutting interactions result when a filament ends on a body. This can occur when filaments are cut by a lifting surface. The cutting of tip vortex filaments by a vertical tail is one example of this type of interaction. A further example occurs when the filaments in a smooth body interaction "pinch-off" with the surface (as described later) and then end on the surfaces. These filaments, which are in a sense cut by the smooth surface, will end on the surface in a perpendicular manner.

Along with classifying the two main types of interaction geometries, each type of interaction can be classified according to the important physical phenomena at work. Essentially, interactions can be viewed as either inviscid or viscous depending on the configuration and stage of development. For example, smooth body interactions begin as inviscid interactions. The three-dimensional distortions that ensue drive a portion of the filament sufficiently near the surface that viscous effects take over and cause the filament to interact with the body boundary layer, and then pinch-off, and split leaving two filaments ending on the surface. The subsequent propagation of the filament end along the surface may then be represented by an inviscid treatment.

The Phase I effort, which was intended as a proof of concept, has dealt with the development of efficient and accurate means to calculate inviscid

vortex dynamics near surfaces. Work on viscous interactions will be undertaken as part of the Phase II effort described later. It is worth noting, however, that the proposed approach to vortex motion for interactional aerodynamics is primarily inviscid. The future study of viscous effects will be targeted to answer certain specific questions, which should allow the modeling and inclusion of such effects within the framework of inviscid vortex dynamics. Since viscous effects act in localized regions, sometimes only briefly, this approach seems appropriate. At the same time, modeling these viscous interactions, which do indeed control the actual splitting or cutting of filaments, is essential to achieving a physically realistic analysis.

The present method uses constant strength curved vortex filaments which are capable of simulating local distortion and rapid changes in curvature, while giving highly accurate near field velocities. The main problem encountered in computing surface interactions will be adequate resolution of the surface panel method. When a vortex filament comes in close proximity with a paneled surface, say when the distance from the surface is less than the panel size, then velocities induced on the filament and on the surface itself will be seriously in error. The most direct approach is to subdivide the surface into many more panels. This requires complex numerical logic and is inefficient. To obtain adequate resolution, it would be necessary to insert panels smaller than the vortex core size, which is much smaller than needed for any other reason. The Phase I effort has developed a much simpler method to correct for close proximity interactions using an analytical solution matched into the numerical flow field.

3.3 Analysis of Smooth Body Interactions

The analytical approach developed in Phase I is best understood by considering the smooth body inteaction problem. To illustrate the expected physical behavior, Figure 20 shows four stages of filament interaction with a smooth surface. As mentioned earlier, a tip vortex filament convected down onto the top of a fuselage or tail boom is one such example. Initially, the filament is convected toward the surface and begins to wrap around it, as

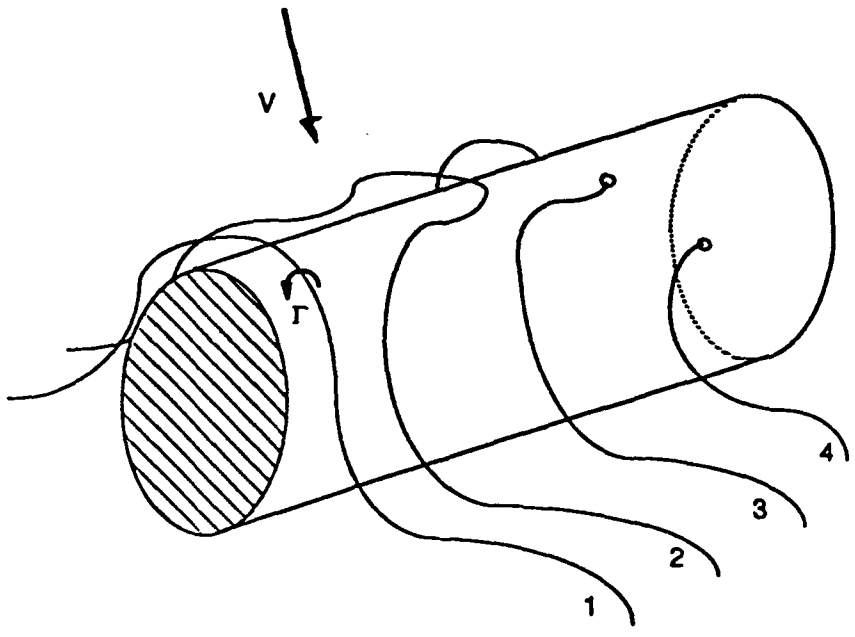

STAGES OF FILAMENT INTERACTION WITH A SMOOTH SURFACE

1. Filament approaches surface.
2. Interaction produces secondary distortion and self-induction towards surface.
3. Filament pinches-off with surface boundary layer.
4. Split filament ends on body sides.

Figure 20. Stages of vortex filament interaction with a smooth surface.

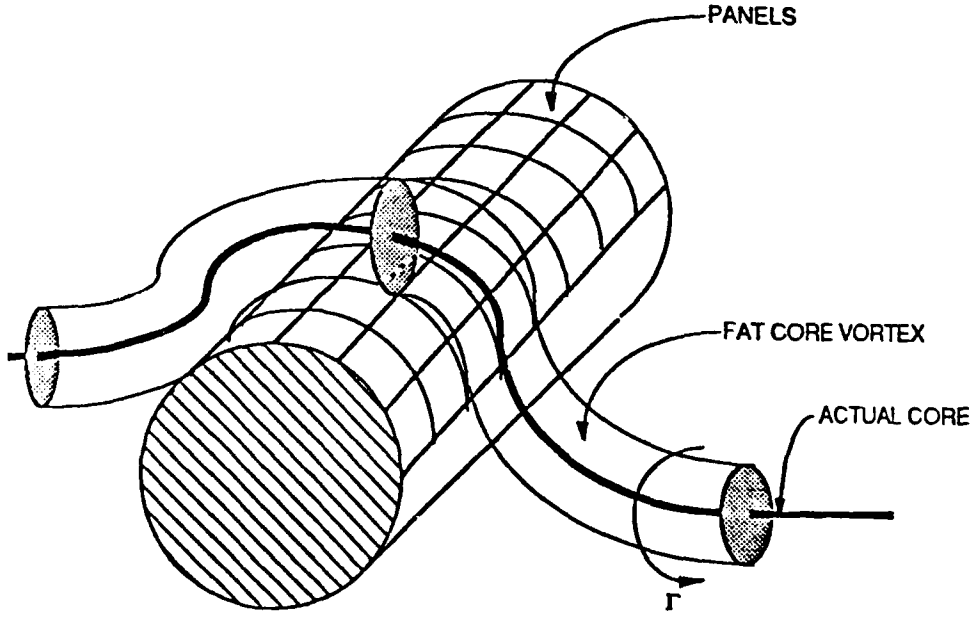

LOW RESOLUTION 3-D SOLUTION: Fuselage Panels See Fat Core

Note: Core size and panel size are comparable.

Figure 21. Schematic of vortex close encounter with a smooth, paneled body.

shown in stage 1 of Figure 20. The effect of the surface is equivalent to the filament interacting with an image filament within the surface. This interaction produces propagation along the surface, with the closest part of the filament having the greatest propagation velocity. This effect leads to a strong secondary stretching and distortion of the filament, as shown in stage 2. The secondary curvature of the filament produces a strong self-induced velocity driving the tip of the distorted region, which has the highest curvature, toward the surface. This leads to a local three-dimensional interaction between the rotational vortex core of the filament and the surface boundary layer. Stage 3 shows that the filament has pinched-off and each half now ends in the surface boundary layer. In stage 4, the smooth body interaction phase is over, and the filaments now are cut by the surface, and their ends convect down around the surface.

Figure 21 shows a numerical representation of the interaction described above in which the body surface is now covered with fairly large aerodynamic panels. As mentioned earlier, resolution problems are encountered when the local distance from the filament to the body is comparable to the panel size, because velocity gradients induced on the surface are then smaller than the spacing between panel control points. To have the paneled surface respond accurately to the presence of the vortex an artifically large vortex core is placed on the filaments to increase the length scale of the local velocity gradients. A core size comparable to or somewhat larger than the panel size is required to achieve this smoothing of the flow field. This filament with the enlarged core is the "fat core vortex" shown in Figure 21. The panels will then give accurate results for this smoothed flow field. Unfortunately, this solution is not acceptable by itself, because it is the correct answer for the wrong vortex core. However, it is possible to develop a local analytical correction to this solution.

Other accuracy simulations of the velocity field near vortex filaments, (e.g., Ref.) have shown that the leading term in the velocity field near a curved vortex is always a two-dimensional line vortex located at the appropriate point along the filament. In general, panel methods must use panel sizes much smaller than the local radius of curvature of the surface to

achieve accuracy. Therefore, a vortex filament at distances from the surface comparable to the panel length will be close enough for the surface to appear relatively flat. As a result, the predominant effects of the local filament/surface interaction will be two-dimensional. This fact allows the construction of a correction solution valid locally which utilizes a two-dimensional vortex above a flat surface. This solution is purely analytical and can be added to the previous three-dimensional fat core vortex to obtain a much more accurate result for the local filament propagation speed and the flow velocities and pressure on the panel surface. The resolution of the local velocities and pressure on the paneled surface is higher than would normally be provided by the panels because of the analytical nature of the local solution.

The analytical local solution is composed of two parts. The first part shown at the top of Figure 22 is a two-dimensional line vortex having the physically correct core size and located above a flat surface. The vortex propagation velocity is parallel to the wall and can be calculated using the image vortex within the wall. This two-dimensional realistic core solution accounts for the local effects of the actual filament. The second part of the local solution is shown at the bottom of Figure 22 which is the two-dimensional near field model of the same fat core filament used in the three-dimensional calculation shown earlier in Figure 21. This part of the two-dimensional solution is used to cancel the local response of the panels to the fat core filament in the three-dimensional calculation. The two-dimensional fat core solution of Figure 22 can be found analytically by an integration of the flat-surface source/sink distribution required to cancel the normal velocity induced on the surface by the fat core vortex. This integral has been carried out for appropriate velocity distributions in the fat core vortex. Note that an image method cannot be used because of the artificial nature of the fat core vortex with its region of rotational fluid extending through the surface.

Using the three-dimensional solution of Figure 21 and the two-dimensional solutions of Figure 22 a composite solution can now be constructed as follows:

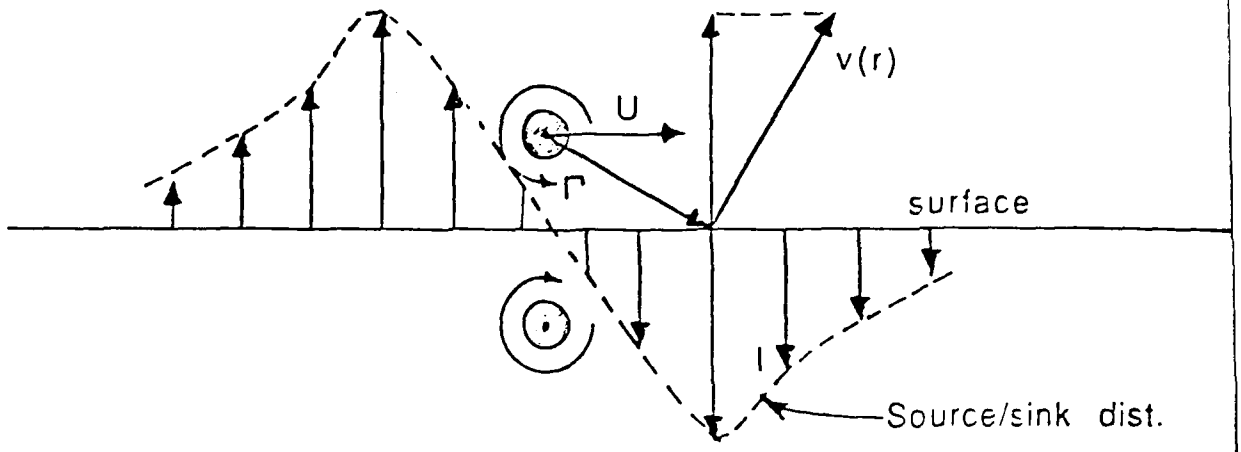

2-D Nearfield Model of Actual Filament

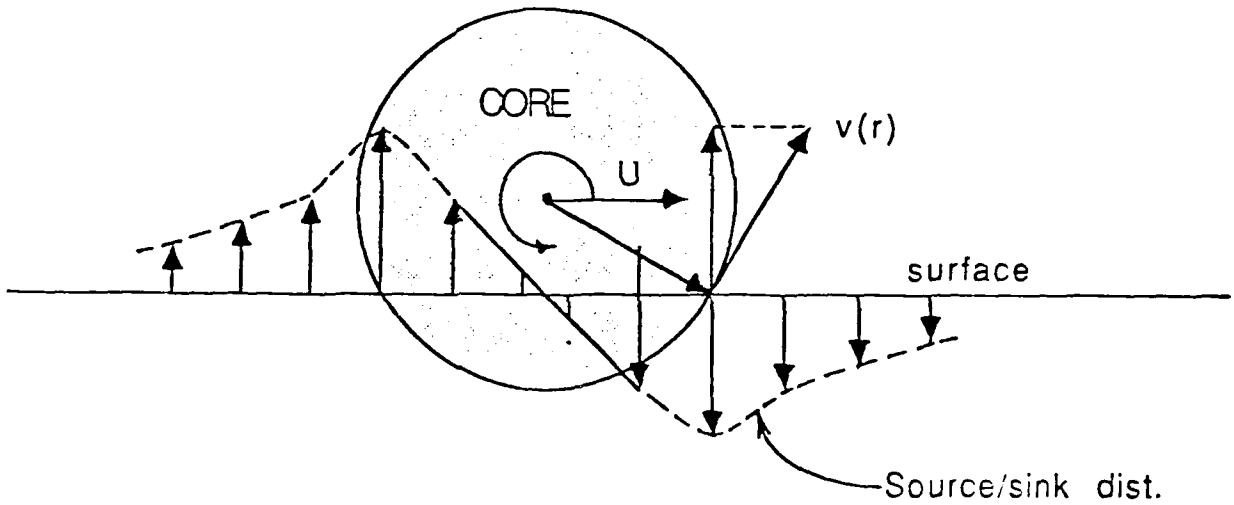

2-D Nearfield Model of Fat-Core Filament

Figure 22. Two-dimensional correction factors to the three-dimensional fat-core solution.

COMPOSITE SOLUTION = 3-D FAT CORE SOLUTION

+ 2-D ACTUAL CORE SOLUTION

- 2-D FAT CORE SOLUTION

In this scheme, the three-dimensional fat core solution accurately accounts for far field and curvature effects. The two-dimensional actual core solutions account for the detailed fine scale structure of the local interaction. The two-dimensional fat core solution cancels the three-dimensional fat core solution near the surface, where is incorrect, and cancels the two-dimensional actual core solution away from the surface where it is incorrect.

The purpose of the approach described above is to allow the accurate simulation of vortex filaments in close proximity to paneled surfaces without resorting to very high panel density. Normally, inaccuracies would result when the filament is less than a panel spacing away from the surface. In the present method a fat core is ficticiously placed around the filament when calculation velocities on a body when calculating velocities on a body in order to smooth gradients on the paneled surface, and an analytical nearfield solution is applied to obtain an accurate answer for the actual core size.

The two-dimensional solutions are important only when the distance to the surface is the order of the fat core radius or smaller. At larger distances they cancel each other, leaving the three-dimensional solution. When the filament is near the surface the local interaction becomes largely two-dimensional. Near the surface the three- and two-dimensional fat core solutions cancel each other, leaving the two-dimensional actual core solution. The approach is similar to the method of Matched Asymptotic Expansions which constructs a composite solution from outer and inner solutions (i.e., composite = outer + inner - inner/outer).

The two-dimensional solutions using the actual and fat cores lead to a relatively simple analytical correction term applied to the vortex convection velocity computed at the filament collocation points. This velocity depends on the distance from the surface, and acts parallel to the surface and perpendicular to the filament. The contribution from the actual core can be calculated by considering its image, but the fat core contribution requires that the source strength distribution to cancel the vortex inflow be integrated over the surface. This correction has been worked out for several possible fat core velocity distributions.

3.4 Solution of Model Problems

The accuracy of this analytical correction to a numerical panel analysis is demonstrated by solving appropriate model problems. The following simple configuration contains relatively few parameters and gives representative results. Figure 23 shows a vortex located above a flat paneled surface. The distance from the surface to the vortex is d, the panel width is ℓ_p, the vortex core size (fat core) is r_c and the off-set between the vortex position and the panel control points is s_o. Distances are normalized by panel width so $\bar{d} = d/\ell_p$, $\bar{r}_c = r_c/\ell_p$ and $\bar{s}_o = s_o/\ell_p$. The correct answer for the vortex horizontal propagation velocity is $u_p = \Gamma/(4\pi d)$ and the correct vertical propagation velocity $v_p = 0$. Computed propagation velocities $\bar{u}$ and $\bar{v}$ are normalized by the correct value of u_p, i.e., $\bar{u} = 1.0$ and $\bar{v} = 0$ is the correct answer.

The swirl velocity around a point vortex is given by

$$v_{exact} = \frac{\Gamma}{2\pi r}$$

The easiest way to construct a corresponding fat core vortex is given by

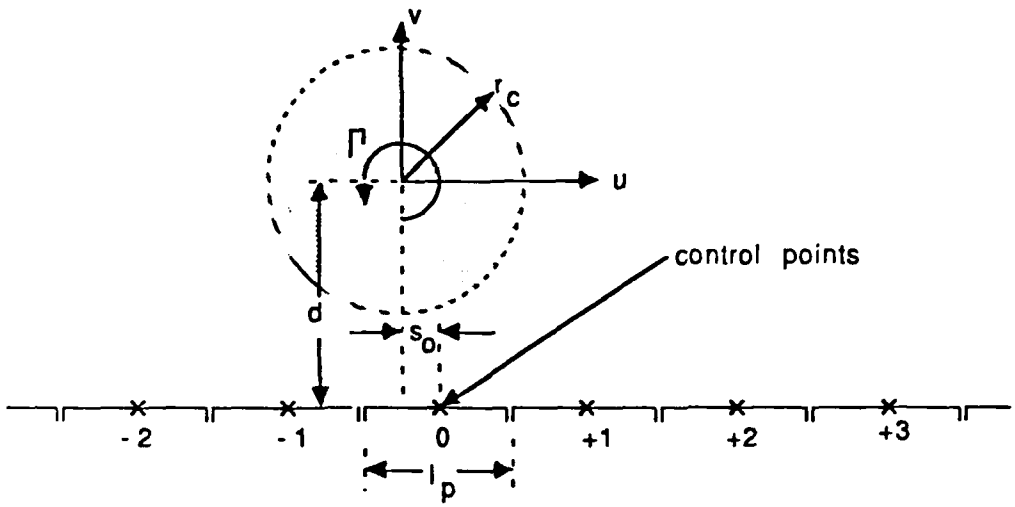

Figure 23. First model problem for assessment of accuracy of analytical correction to panel method: vortex over a flat surface.

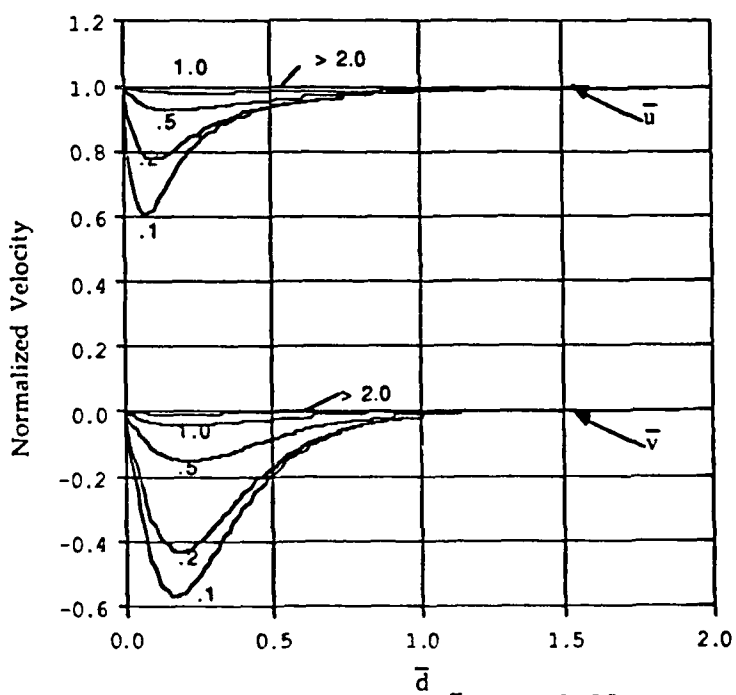

a) Offset distance $\bar{s}_o = -0.25$.

Figure 24: Vortex near a flat surface: nondimensional velocities $\bar{u}$ and $\bar{v}$ versus distance from the surface for various r_c .

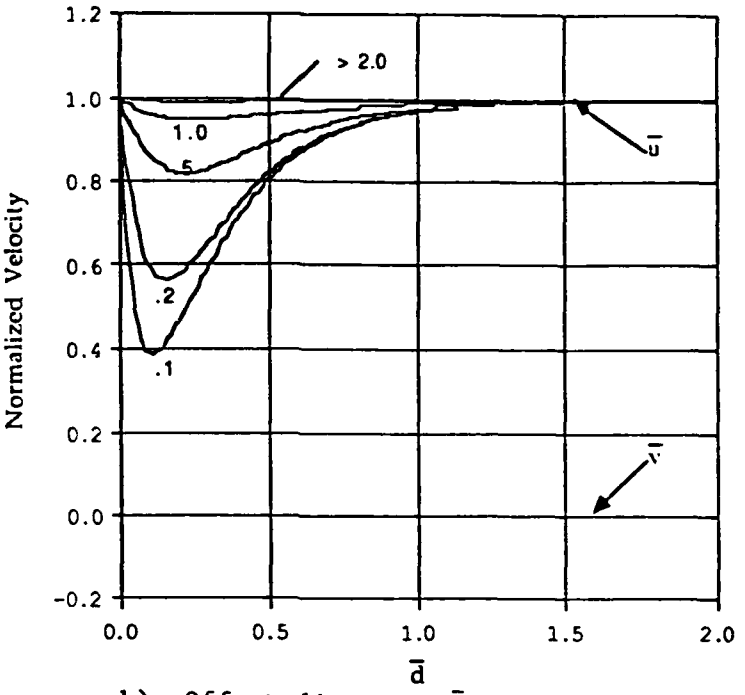

b) Offset distance $\bar{s}_o = 0.0$.

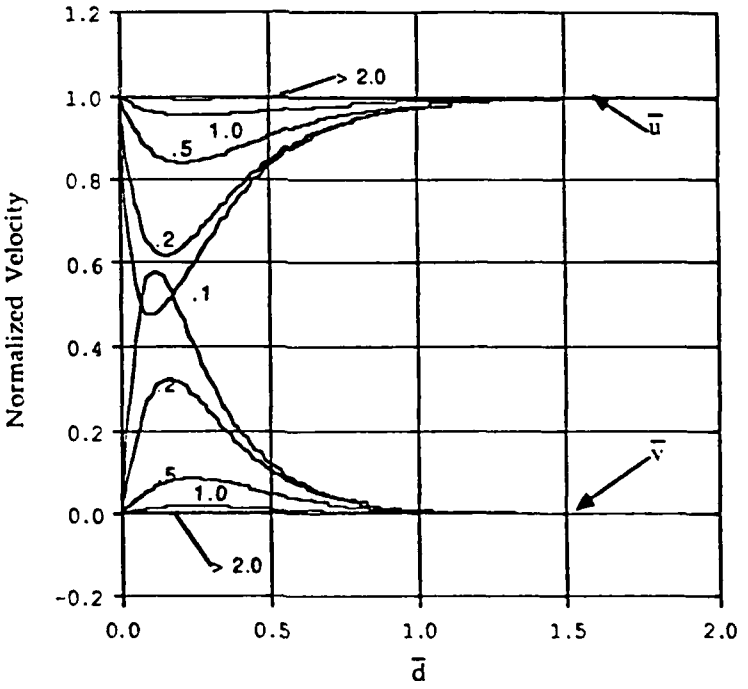

c) Offset distance $\bar{s}_o = 0.1$.

Figure 24 (Cont'd): Vortex near a flat surface: non-dimensional velocities $\bar{u}$ and $\bar{v}$ versus distance $\bar{d}$ from the surface for various $\bar{r}_c$.

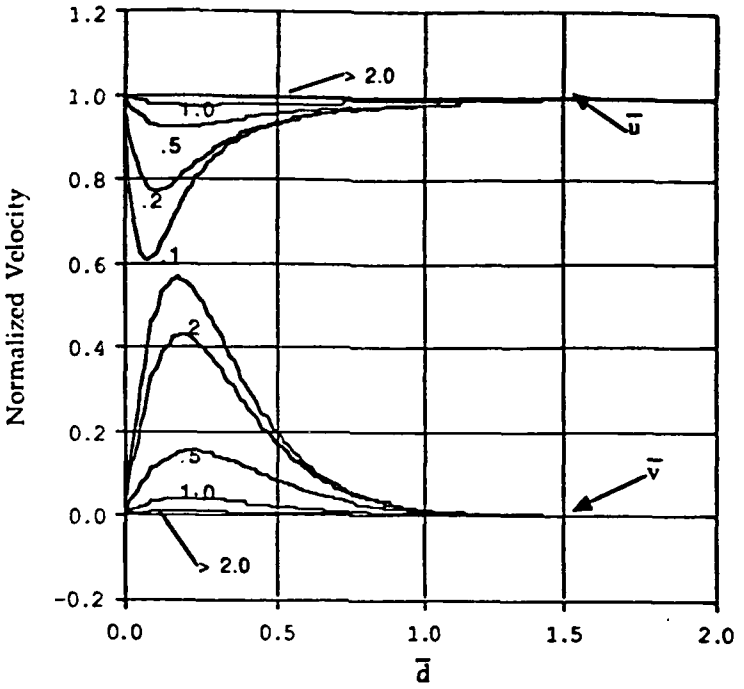

d) Offset distance $\bar{s}_o = 0.25$.

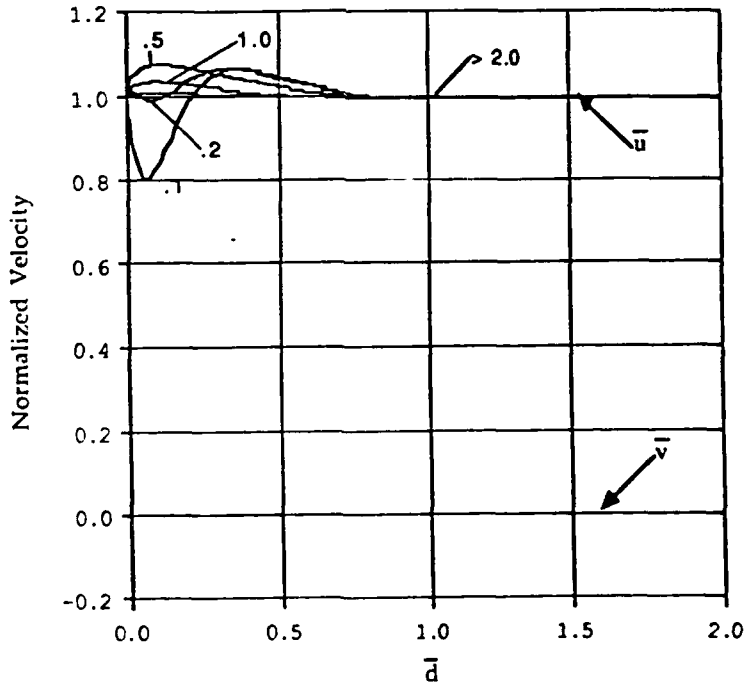

e) Offset distance $\bar{s}_o = 0.5$.

Figure 11 (Cont'd): Vortex near a flat surface: nondimensional velocities $\bar{u}$ and $\bar{v}$ versus distance from the surface for various $\bar{r}_c$.

$$v_{\text{fat core}} = \frac{\Gamma}{2\pi} \frac{r}{r^2 + r_c^2}$$

where r_c is the core size length scale. For $r < r_c$ the swirl velocity approaches solid body rotation, and for $r > r_c$ the swirl velocity approaches the point vortex behavior given above. When $r = r_c$ the swirl velocity takes on its maximum value. The velocity induced on the point vortex above the surface is $u_{p_{exact}} = \Gamma/4\pi d$. A more involved calculation, which treats the surface as a distributed source distribution, gives the velocity induced on the local fat core as

$$u_{p_{\text{fat core}}} = \frac{\Gamma}{4\pi d} \frac{2d}{d + \sqrt{d^2 + r_c^2}}$$

When $r_c << d$ the point vortex result is recovered. The expression for $u_{p_{exact}}$ serves as the two-dimensional core solution, and the expression for $u_{p_{\text{fat core}}}$ is the two-dimensional actual core solution. The outer fat core solution is generated numerically using constant strength source panels. These three solutions are combined to form the composite solution as described previously.

Sample calculations were carried out to test the accuracy of the composite solution described earlier as applied to this case. A sequence of results is shown in Figure 24a, b, c, d, and e which shows the computed normalized velocities $\bar{u}$ and $\bar{v}$ as a function of normalized distance $\bar{d}$ of the vortex above the paneled surface. Each plot has a fixed collocation point off-set s_o relative to the vortex. On a given plot different curves signify the results for different values of the normalized vortex core $\bar{r}_c$. Since the actual core may be much smaller than a panel size, curves for small values of $\bar{r}_c$, say 0.1 and 0.2, are representative of the types of errors that may be encountered if the actual filament were allowed to come near a paneled surface. Within one panel width from the wall, namely $\bar{d} < 1$, very large errors are encountered and filament motion would not be predicted accurately. On the other hand, when larger values of the fat core are used, the

analytical correction procedure comes into play and the errors are quickly diminished to negligible values as $\bar{r}_c$ is increased. On the plots shown, $\bar{r}_c > 2.0$ consistently gives good accuracy for both $\bar{v}$ and $\bar{u}$ for all values of $\bar{s}_o$. This shows that the fat core radius needs to be approximately twice the panel size. Finally, comparisons between the various plots in Figure 24a, b, c, d, e, shows the strong dependence on $\bar{s}_o$, the relative offset between the vortex and the panel control points. Introducing the analytical correction procedure with $\bar{r}_c > 2.0$ removes this spurious dependence. These results show both the inadequacy of using a standard panel method with a free wake analysis, and illustrate the effectiveness of the analytical correction procedure developed under the Phase I effort.

A second model problem was also studied to test the method treating vortex/surface interactions under more realistic circumstances. Figure 25 shows a point vortex in close proximity to a circular cylinder represented by linear vortex panels. The radius of curvature, R, of the cylinder is an additional parameter not present in the previous simulation. This model problem allows the effect of curvature to be assessed. The analytical solution for a point vortex next to a cylinder can be readily calculated using the circle theorem.

Parameters were again nondimensionalized in a manner analogous to the previous model problem, using the same notation. Lengths are nondimensionalized with panel length ℓ_p. The angular offset of the point vortex relative to the panel control point is given by θ_d. When the vortex is directly above the junction between two panels $\theta_d = \theta_p/2$, where θ_p is the included angle of one panel on the cylinder surface. Nondimensionally, this offset is denoted by $s = \theta_d/\theta_p$, in close analogy to the offset parameter, s, in the previous model problem. Velocities are nondimensionalized with the exact tangential propagation velocity of the vortex around the cylinder, with the net circulation around the cylinder set equal to that of the point vortex. Although the circulation around the cylinder can be specified arbitrarily, this particular choice recovers the results of the previous model problem when R approaches infinity.

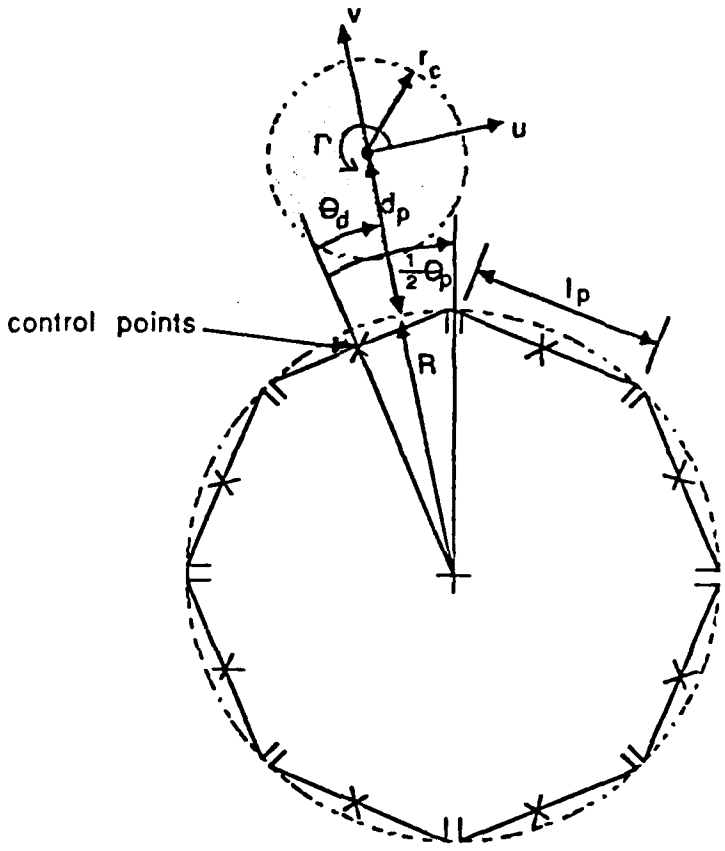

Figure 25: Second model problem: vortex near a cylinder (using inner solution with curvature).

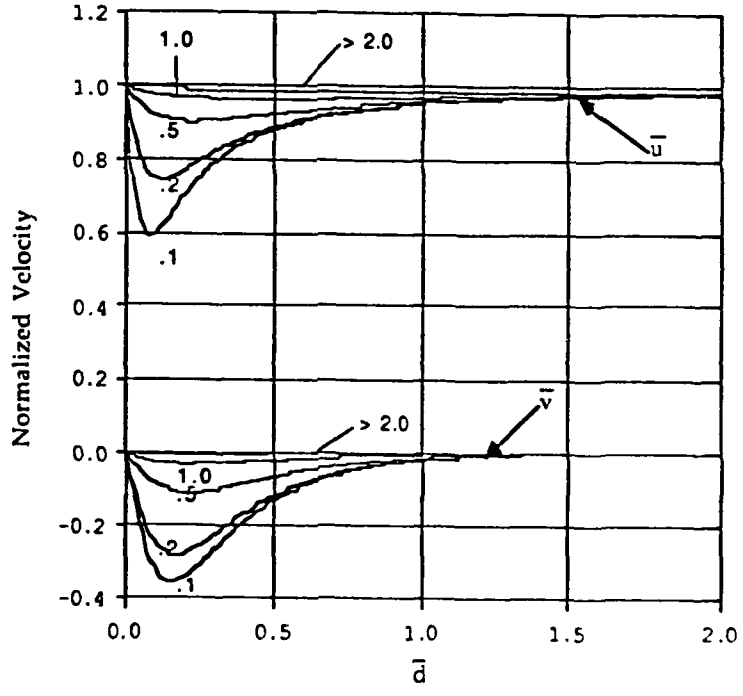

a) Offset distance $\bar{s}_o = -0.25$.

Figure 26: Vortex near a cylinder (using inner solution with curvature): [illegible] the surface for various $\bar{r}_c$.

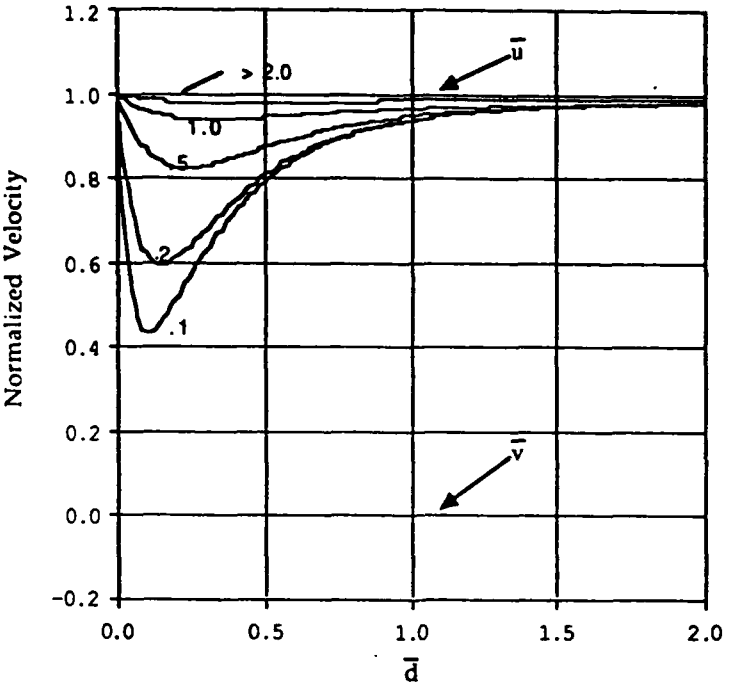

b) Offset distance $\bar{s}_o = 0.0$.

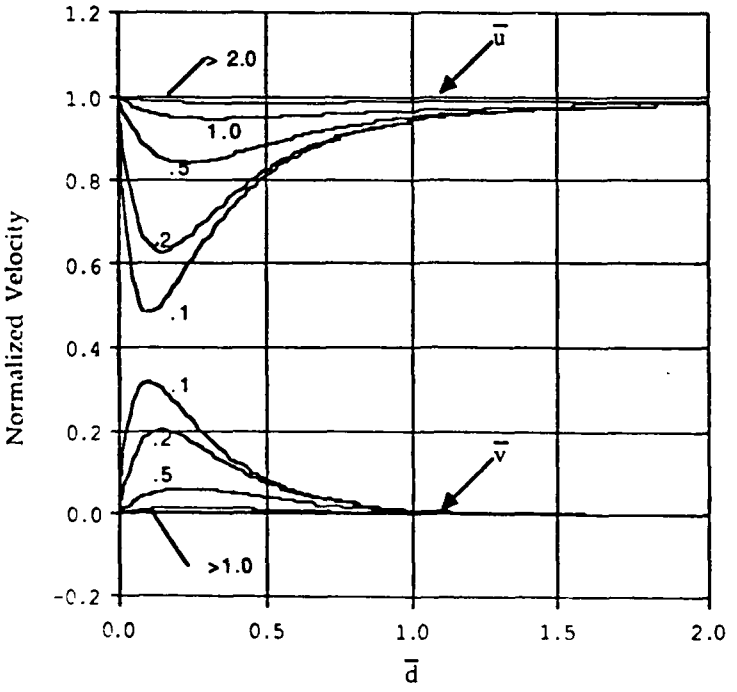

c) Offset distance $\bar{s}_o = 0.1$.

[illegible]: Vortex near a cylinder (using linear solution with curvature): [illegible] solutions $\bar{u}$ and $\bar{v}$ versus distance from the surface for various $\bar{r}_c$.

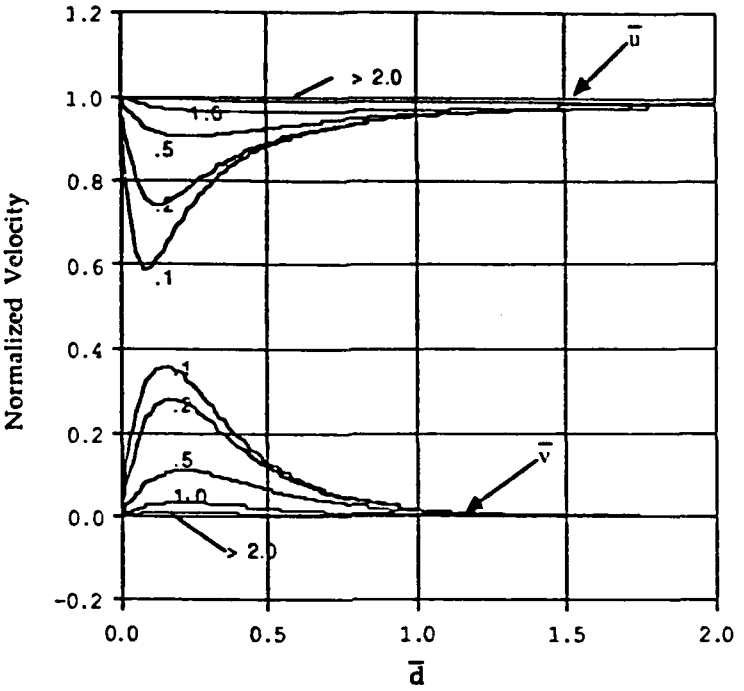

d) Offset distance $\bar{s}_o = 0.25$.

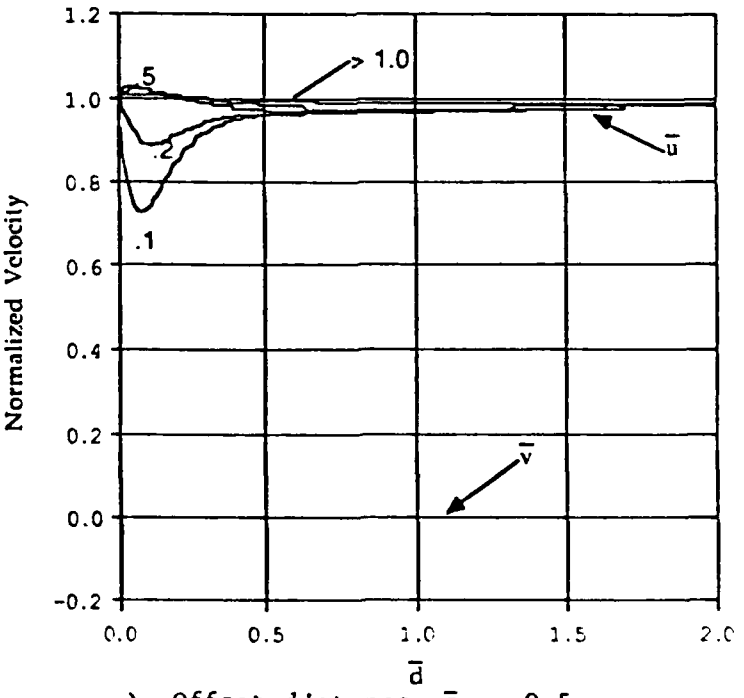

e) Offset distance $\bar{s}_o = 0.5$.

Figure 26 (Cont'd): Vortex near a cylinder (with finer resolution with curvature): Nondimensional velocities $\bar{u}$ and $\bar{v}$ versus distance from the surface for various $\bar{r}_c$.

In order to study local curvature effects, two different sets of inner (two-dimensional actual core) and inner-outer (two-dimensional fat core) solutions were used for this model problem. The more accurate set was based on exact solutions for a point vortex and fat core vortex in the presence of a cylinder. The point vortex case was obtained analytically using the circle theorem, and the exact fat core case was obtained numerically (primarily as an expedient). Although the present model problem involves a cylinder, these same local solutions are also applicable to any other curved body shape simply by using the local radius of curvature. The other set of local solutions were taken from the first model problem and involve only a flat surface in the inner region.

Figure 26 shows a set of calculations for the model problem of a vortex near a cylinder. The calculations were made for the more precise near field solutions with curvature. The cylinder is represented by 12 linear vortex panels, which is a relatively low panel density, especially considering the large local gradients generated by the vortex. The sequence of cases for different values of the offset parameter, s, are shown in parts a, b, c, d and e of Figure 26, and correspond exactly to the same parts in Figure 24. In fact, the results are quite similar and the same comments and observations made earlier in reference to Figure 24 apply equally to Figure 26. However, the general conclusion should be restated: very accurate results are obtained consistently by using a fat core size, r_c, that is twice the panel size. In fact, even r_c equal to ℓ_p never gives an error greater than a few percent, and excellent level of accuracy for interactional aerodynamics calculations.

A detailed comparison of Figures 24 and 26 for the two model problems shows only minor differences. For a given core size, the tangential velocities, $\bar{u}$, are nearly identical, but the normal velocities, $\bar{v}$, often show smaller errors for the cylinder simulation. Actually, this difference is very likely due to the different choice of panel methods in the two cases. The linear vortex panels used for the cylinder simulation have higher order accuracy in comparison to the constant strength source panels used for the flat surface model problem. Consistent with this fact, it can be shown that the normal velocity is more sensitive than the tangential velocity to the

effect of the nearest panels. Since both panel methods work well for a sufficiently large fat core size, the important point is that the new method for handling vortex/surface interactions is relatively insensitive to the type of panel method, and to its order of accuracy.

Figure 27 shows the same set of calculations as Figure 26, except that the local solutions (two-dimensional actual core and two-dimensional fat core) treat the surface as flat, as in the first model problem. Comparison of the corresponding cases in Figures 26 and 25 (for the same values of offset parameter s) shows that neglecting curvature leads to slightly larger errors when the fat core size is small. Velocity errors no greater than a few percent are obtained consistently when the fat core size equals the panel size. However, for larger fat core sizes a different trend occurs, with the tangential velocity error changing sign and increasing slightly. This effect occurs because the fat core extends beyond the region where the flat and curved surfaces nearly coincide. As a result, there are residual differences between the inner and outer solutions in the overlap region. The result is noticeable only in the tangential velocity because this component is sensitive to the effects of panels farther from the vortex. The best results, which occur when the core size equals the radius of curvature, are actually due to cancelling error terms. This behavior shows that when the surface is modeled as flat in the inner solution, the choice of fat core size for good accuracy depends weakly on the radius of curvature, in addition to its strong dependence on panel size. Introducing local curvature into the inner solution effectively removes this dependence. It should be noted, however, that the only reason this effect is seen is because only twelve panels were used to represent the cylinder. However, even in this case the flat inner region gives results of acceptable accuracy for most interactional aerodynamics problems.

To explore the effect of number of panels, calculations with the cylinder represented as few as six panels, and as many as twelve panels, was conducted for offset parameter $s = 0.25$, which gave fairly large errors in the earlier simulations. Figure 28 shows a comparison of results for a cylinder represented by six, twelve, twenty-four, and infinitely-many panels (the

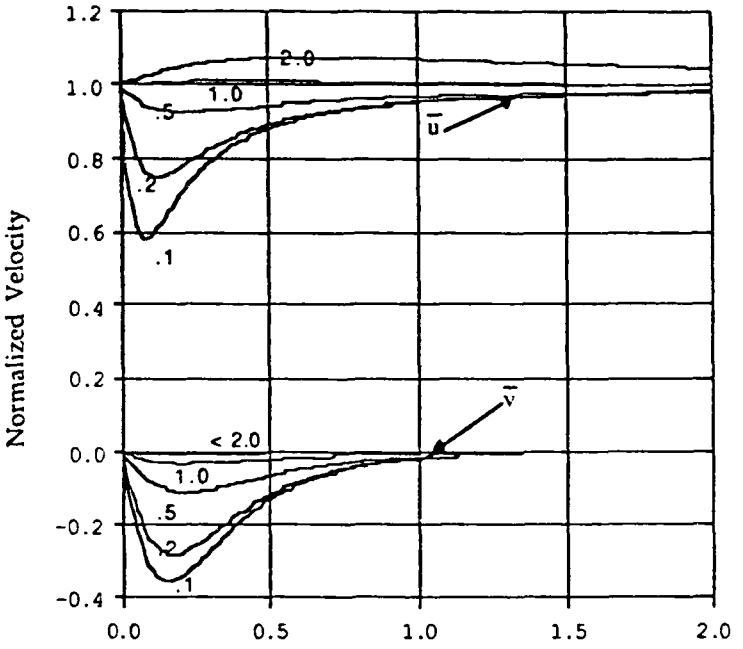

a) Offset distance $\bar{s}_o = -0.25$.

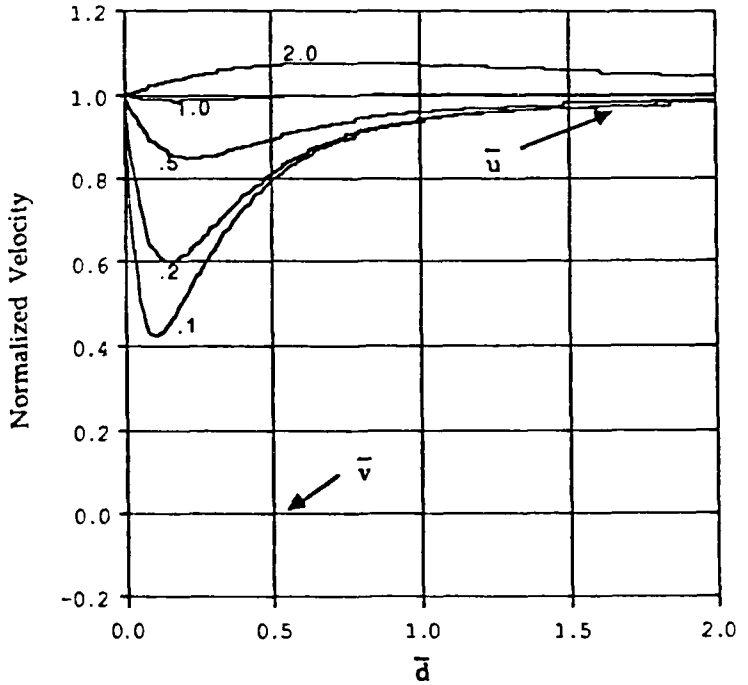

b) Offset distance $\bar{s}_o = 0.0$.

Figure 27: Vortex near a cylinder (using flat surface inner solution): nondimensional velocities $\bar{u}$ and $\bar{v}$ versus distance from the surface for various $\bar{r}_c$.

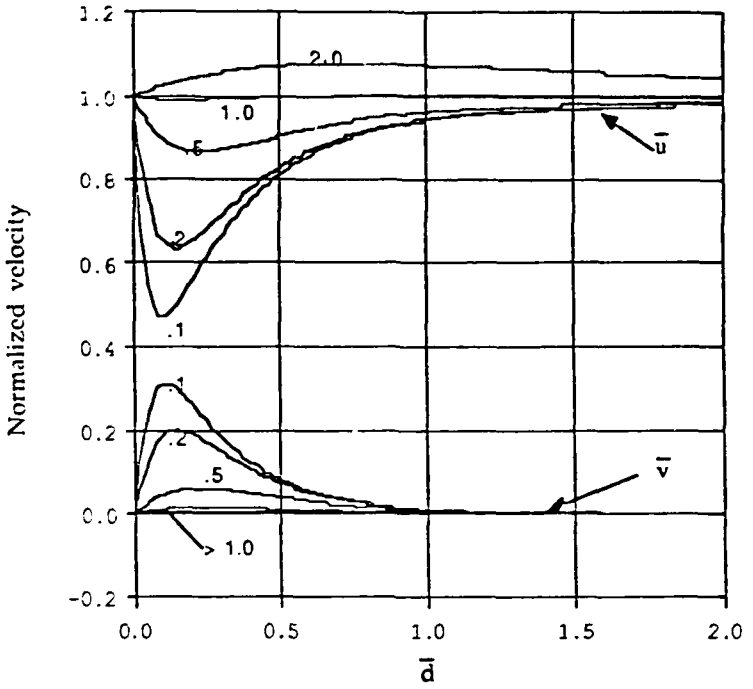

c) Offset distance $\bar{s}_o = 0.1$.

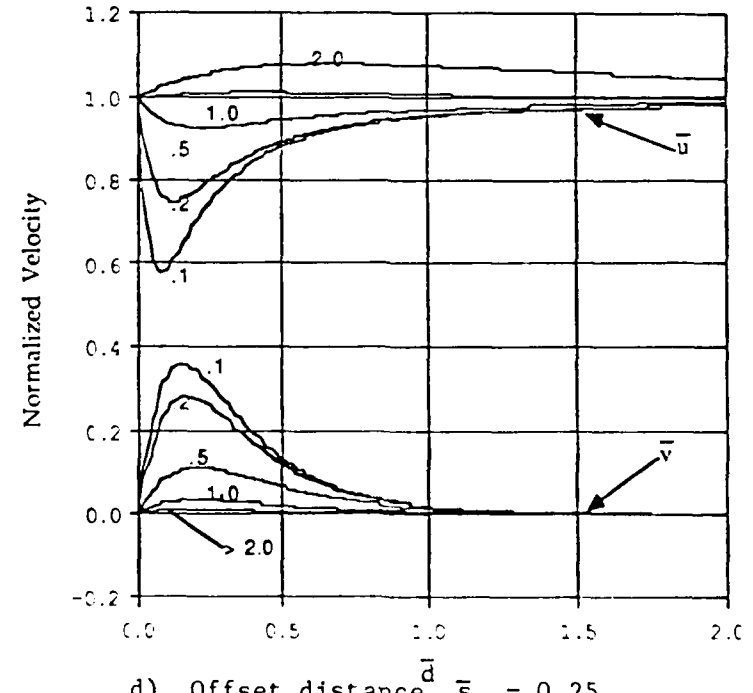

d) Offset distance $\bar{s}_o = 0.25$.

[illegible] inner solution): [illegible] distance from the surface [illegible] .

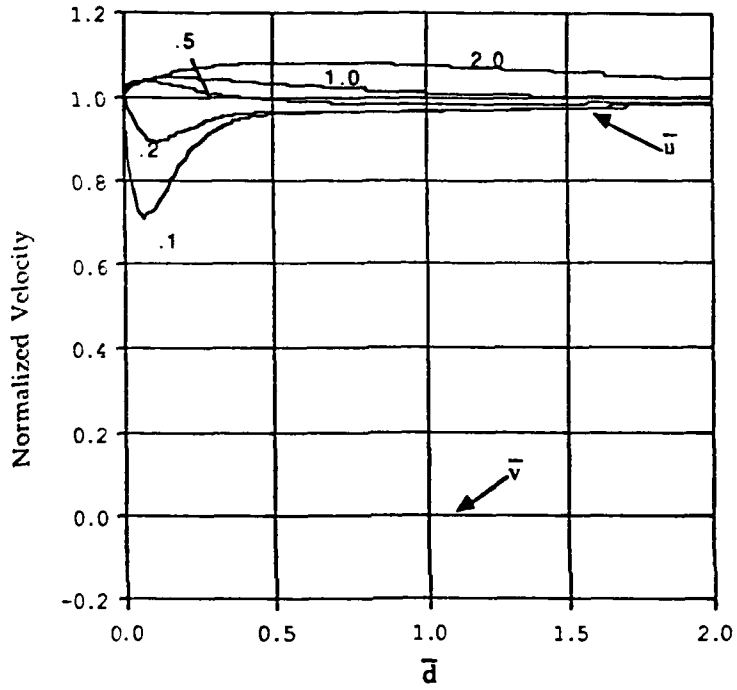

e) Offset distance $\bar{s}_o = 0.5$.

Figure 27 (Cont'd): Vortex near a cylinder (using flat surface inner solution): nondimensional velocities $\bar{u}$ and $\bar{v}$ versus distance from the surface for various $\bar{r}_c$.

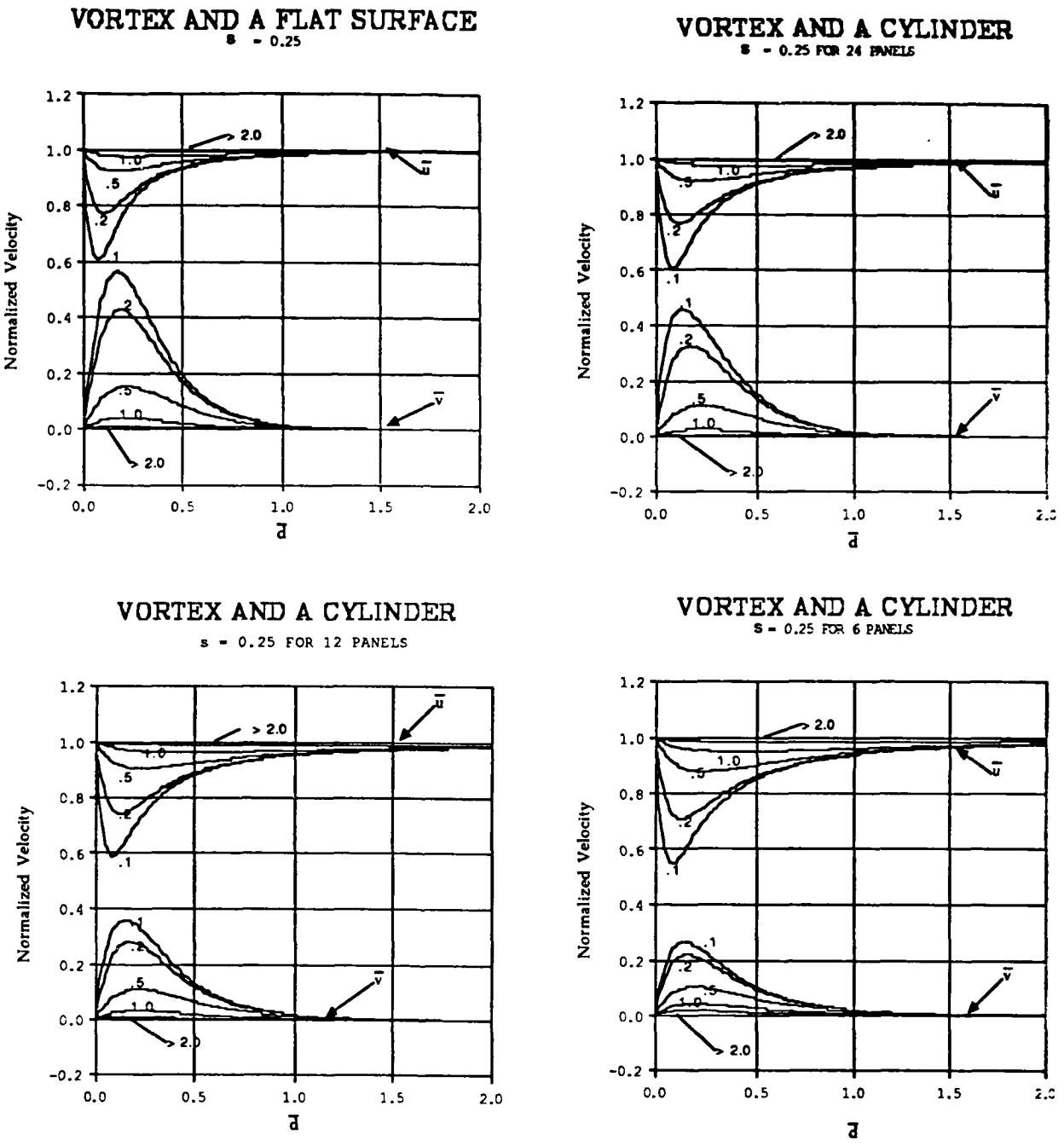

Figure 28: Effect of number of panels on the velocity components induced on a vortex above a cylinder.

latter case is just the flat surface simulation). Because the problem is nondimensionalized with the panel length, as the number of panels increases with all other parameters held fixed, it is as if the cylinder radius, R , is increasing to accommodate the increasing number of panels. Note that the cases with a finite number of panels use the curved inner solutions of the second model problem, which improves the results at low panel density. The fact that very good results were still obtained for only six panels indicates the effectiveness, and efficiency, of the method.

The primary conclusion of the model problem study is that the new method for handling smooth-body vortex/surface interactions works extremely well. Close proximity interactions are handled extremely well, even for very low panel densities. The extension of this method to handle three-dimensional outer flow fields is clearly feasible, and hold enormous promise as a new accurate method to perform interactional aerodynamics calculations in a physically correct and realistic manner.

3.5 Cutting Interactions

In addition to smooth body interactions, an accurate inviscid treatment of vortex cutting interactions on paneled surfaces is also under consideration. As mentioned before, rotor wake filaments cut by lifting surfaces such as the empennage or stabilizer are common examples of this type of interaction. Furthermore, rotor wake filaments that end on smooth surfaces, after pinch-off and splitting as described earlier, also belong to this class of interactions. There are two important issues in the case of inviscid cutting interactions: the proper termination of the vortex at the surface and the correction of discretization errors due to surface paneling.

The vortex terminating on the surface sees its mirror image extending into the surface. To avoid a singularity due to kinking vortex lines, it is necessary that the vortex filament tangent vector be normal to the surface at the point of intersection. The point where the filament intersects the surface is convected along the surface by several effects. In addition to the

local surface velocity in the absence of the vortex, the filament responds to velocities induced by its interaction with the surface, and by local self-induction due to filament curvature at the surface.

An approach very similar to the previous method can be used to model the cutting interaction. An artificially enlarged core is used to smooth gradients on the paneled surface, as shown in Figure 29. An analytical quasi-two-dimensional correction is developed to obtain the correct answer. An important difference in the present case is that the self-induction effect must be handled correctly, since it comes in part from the response of the paneled surface to the enlarged core. This is not a two-dimensional effect so an additional analytical correction for self-induction is required.

The analytical correction in this case can be visualized as two coincident circular arcs, one with the realistic core size and positive circulation and one with the fat core and negative circulation. Both circular arcs must leave the paneled surface at the same point and have the same radius of curvature as the actual filament at the intersection point. These arcs must extend an equal distance above the surface, far enough so that the fat core at the upper end no longer intersects the surface. Beyond this point the circular arcs cancel, leaving the correct far field due to the actual wake filament. In the near field, the fat core circular arc cancels the fat core wake filament and the near field panel response to this filament, leaving the correct contribution of the circular arc with the realistic core. Since the circular arc velocities are only needed relatively near the arc (namely within the fat core region) these effects can be obtained analytically by an expansion method. A similar approach to obtain velocites has been used previously in accuracy studies of the near field of curved vortex filament, Ref. 4 and in the analysis of self-induced motion of curved rotational vortex filaments, Ref. 21. The composite solution for cutting interactions is then as follows:

COMPOSITE SOLUTION = 3-D FAT CORE SOLUTION

+ ACTUAL CORE CIRCULAR ARC

- FAT CORE CIRCULAR ARC

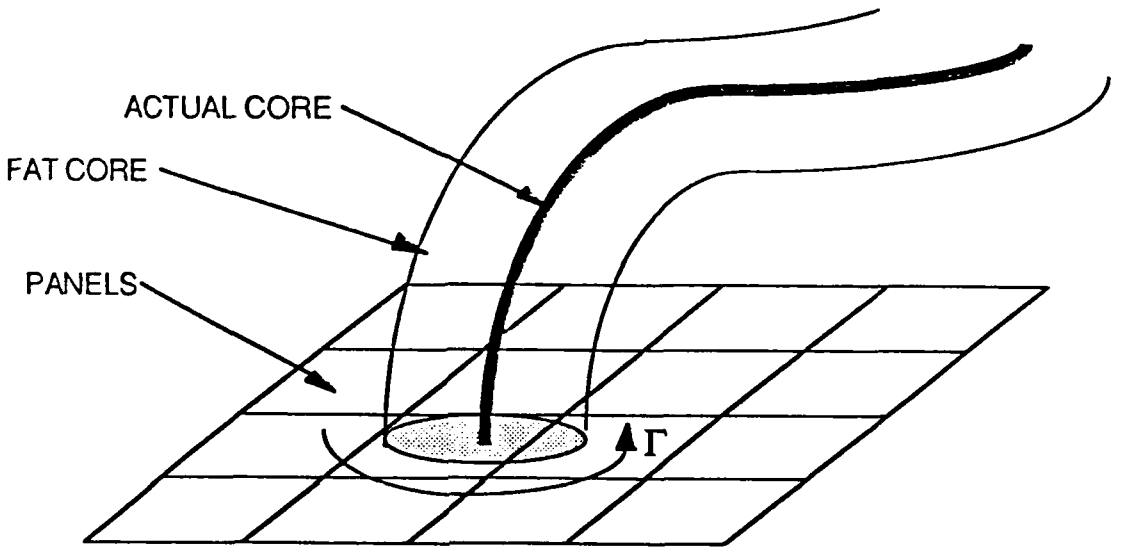

Figure 29: Vortex filament ending on a paneled surface.

Except for the need to use circular arcs to pick up the curvature effect at the surface this approach is conceptually similar to the smooth surface interaction correction discussed earlier.

4. CONCLUSIONS

The fundamental objective of this Phase I effort has been to demonstrate the feasibility of applying recent innovations in the study of vortex dynamics to the analysis of rotorcraft interactional aerodynamics. By incorporating a recently-developed full-span rotor wake model into a simulation of the flow downstream of the rotor, good qualitative and quantitative agreement with induced velocity data has been achieved for both low- and high-speed cases. In particular, the complex flow field downstream of a rotor in high-speed forward flight has been correlated with good accuracy. Such accurate predictions of wake-induced velocities is a crucial first step in the treatment of interactional aerodynamics, since these velocities govern the forcing experienced by surfaces downstream. As noted in the discussion of major interactional mechanisms in Section 2, the nature of this forcing has been shown to vary dramatically depending on the forward speed of the helicopter.

In addition to the implementation of novel wake models for the study of downwash and sidewash, new departures in the treatment of vortex/surface interaction have been described. The model problems discussed in Section 3 have demonstrated the flexibility and robustness of the new interaction method, which obviates the need for elaborate schemes for local repaneling of downstream surfaces operating in vortex-dominated flow fields. The discussion above has not only presented the substance of the new smooth-body interaction treatment, but has also outlined an analagous treatment for filaments undergoing cutting interactions with surfaces.

It is clear, however, that considerable enhancements to the capabilities described in this report are required to produce a generally applicable interactional aerodynamics analysis. The proposed schemes for cutting interactions must be implemented and new methods for modeling the effect of local viscous interactions in the context of an overall inviscid analysis must be developed. In addition, account must be taken of the presence of the wake of nonlifting components such as the rotor hub, and all of these new features

must be coupled to an appropriate panel method analysis for rotorcraft surface loads. However, the successful development of the inflow prediction techniques described herein, taken together with the new methods of treating close vortex/surface encounters, has laid the foundation for a general analysis of rotor/airframe interaction.

REFERENCES

1. Miller, R.H.: "Rotor Blade Harmonic Air Loading," AIAA Journal, July 1964.

2. Egolf, T.A. and Landgrebe, A.J.: "Helicopter Rotor Wake Geometry and Its Influence in Forward Flight," Vols. I and II, NASA CR 3726 and 3727, October 1983.

3. Scully, M.P.: "Computation of Helicopter Rotor Wake Geometry and Its Influence on Rotor Harmonic Airloads," MIT ASRL TR 178-1, March 1975.

4. Bliss, D.B., Teske, M.E. and Quackenbush, T.R.: "A New Methodology for Free Wake Analysis Using Curved Vortex Elements," NASA CR 3958, 1987.

5. Quackenbush, T.R., Bliss, D.B. and Wachspress, D.A.: "Preliminary Development of an Advanced Free Wake Analysis of Rotor Unsteady Airloads," Continuum Dynamics, Inc. Report No. 87-6 prepared as an SBIR Phase I Report for NASA/Ames under Contract No. NAS2-12554, August 1987.

6. Weisner, W. and Kohler, G.: "Tail Rotor Performance in the Presence of Main Rotor, Ground, and Winds," presented at the 29th Annual Forum of the American Helicopter Society, May 1973.

7. Sheridan, P.F.: "Interactional Aerodynamics of the Single Rotor Helicopter Configuration." USARTL TR-78-23A, Vol. I, September 1978.

8. Sheridan, P.F., Hanker, E.J. and Blake, B.B.: "Investigation of Operational and Design Factors Resulting from Main Rotor and Tail Rotor Interactions." USAAVRADCOM TR-82-D-40, November 1983.

9. Blake, B.B., Hodder, D.S. and Hanker, E.J.: "Wind Tunnel Investigation Into the Directional Control Characteristics of an OH-58A Helicopter." USAAVRADCOM TR-83-D-18, June 1984.

10. Prouty, R. and Amer, K.B.: "The YAH-64 Empennage and Tail Rotor - A Technical History," presented at the 38th Annual Forum of the American Helicopter Society, April 1982.

11. Gangwani, S.T.: "Calculations of Rotor Wake Induced Empennage Airloads," Journal of the American Helicopter Society, April 1983.

12. Egolf, T.A. and Lorber, P.F.: "An Unsteady Rotor/Fuselage Interaction Method." Proceedings of the American Helicopter Society National Specialist's Meeting on Aerodynamics and Aeroacoustics, February 1987.

13. Rand, O.: "The Influence of Interactional Aerodynamics in Rotor/Fuselage Coupled Response," presented at the 2nd International Conference on Rotorcraft Basic Research, University of Maryland, College Park, Maryland, February 1988.

14. Berry, J.D.: "Prediction of Time-Dependent Fuselage Pressures in the Wake of a Helicopter Rotor," presented at the 2nd International Conference on Rotorcraft Basic Research, University of Maryland, College Park, Maryland, February 1988.

15. Clark, D. and Maskew, B.: "Calculation of Unsteady Rotor Blade Loads and Blade Fuselage Interference," presented at the 2nd International Conference on Rotorcraft Basic Research, University of Maryland, College Park, Maryland, February 1988.

16. Quackenbush, T.R.: "Computational Studies in Low-Speed Rotor Aerodynamics," Ph.D. Thesis, Princeton University Department of Mechanical and Aerospace Engineering, September 1986.

17. Heyson, H.H. and Katzoff, S.: "Induced Velocities Near a Lifting Rotor with Nonuniform Disk Loading." NACA Report No. 1319, 1957.

18. Logan, A.H., Prouty, R.W. and Clark, D.R.: "Wind Tunnel Tests of Large- and Small-Scale Rotor Hubs and Pylons." USAAVRADCOM TR-80-D-21, April 1981.

19. Prouty, R.W.: "The Importance of Aerodynamics on Handling Qualities." Proceedings of the American Helicopter Society National Specialist's Meeting on Aerodynamics and Aeroacoustics, February 1987.

20. Baskin, V.Ye., Vil'dgrube, L.S., Vozhdayey, Ye.S. and Maykapar, G.I.: "Theory of Lifting Airscrews." NASA TTF-823, 1975.

21. Bliss, D.B.: "Prediction of Tip Vortex Self-Induced Motion Parameters in Terms of Rotor Blade Loading," proceedings of the American Helicopter Society National Specialists' Meeting in Aerodynamics and Aeroacoustics, February 1987.